

REPORT DOCUMENTATION PAGE

Form Approved OMB No. 0704-0188

Public reporting burden for this collection of information is estimated to average 1 hour per response, including the time for reviewing instructions, searching existing data sources, gathering and maintaining the data needed, and completing and reviewing the collection of information. Send comments regarding this burden estimate or any other aspect of this collection of information, including suggestions for reducing the burden, to Department of Defense, Washington Headquarters Services, Directorate for Information Operations and Reports (0704-0188), 1215 Jefferson Davis Highway, Suite 1204, Arlington, VA 22202-4302. Respondents should be aware that notwithstanding any other provision of law, no person shall be subject to any penalty for failing to comply with a collection of information if it does not display a currently valid OMB control number.
PLEASE DO NOT RETURN YOUR FORM TO THE ABOVE ADDRESS.

1. REPORT DATE (DD-MM-YYYY) 03-09-2007	2. REPORT TYPE Interim Report	3. DATES COVERED (From – To) 1 May 2007 - 3-Sept-07
--	---	---

4. TITLE AND SUBTITLE Solar Wind driven autoregression model for Ionospheric short term Forecast (SWIF).	5a. CONTRACT NUMBER FA8655-07-M-4008
	5b. GRANT NUMBER
	5c. PROGRAM ELEMENT NUMBER

6. AUTHOR(S) Dr. Anna Belehaki	5d. PROJECT NUMBER
	5d. TASK NUMBER
	5e. WORK UNIT NUMBER

7. PERFORMING ORGANIZATION NAME(S) AND ADDRESS(ES) Ionospheric Group, Institute for Space Applications and Remote Sensing, Metaxa and Vas. Pavlou str. Palaia Penteli 15236 Greece	8. PERFORMING ORGANIZATION REPORT NUMBER N/A
---	--

9. SPONSORING/MONITORING AGENCY NAME(S) AND ADDRESS(ES) EOARD PSC 821 BOX 14 FPO AE 09421-0014	10. SPONSOR/MONITOR'S ACRONYM(S)
	11. SPONSOR/MONITOR'S REPORT NUMBER(S) SPC 07-4008

12. DISTRIBUTION/AVAILABILITY STATEMENT
Approved for public release; distribution is unlimited.

13. SUPPLEMENTARY NOTES

14. ABSTRACT

This report results from a contract tasking Ionospheric Group, Institute for Space Applications and Remote Sensing, as follows: The grantee will investigate the development of an end-to-end short-term (up to 24 hours ahead) ionospheric prediction service, SWIF, based on a fusion of two diverse techniques: (1) an autoregression forecasting algorithm capable for real time predictions and (2) an empirical model (STIM) for predicting the onset and for scaling ionospheric disturbances during geomagnetic storms based on the solar wind parameters. The service will be applied for Athens location, by utilizing Athens Digisonde observations. Moreover, the predictions of the new algorithm will be evaluated in terms of both real observations and GCAM predictions for various ionospheric conditions and possible limitations of each method will be determined. The comparative evaluation of ionospheric prediction methods based on techniques of different approach would provide significant progress towards the accurate specification and forecasting of the evolution of ionospheric irregularities over Europe, which has a major impact on defense interests. In summary, the objectives of this project are: 1. development of the SWIF model 2. evaluation of the performance of the SWIF model in comparison to the results of other ionospheric models 3. on line demonstration of the SWIF model performance.

15. SUBJECT TERMS
EOARD, Space Environment, Earth Sciences, Solar Physics

16. SECURITY CLASSIFICATION OF:			17. LIMITATION OF ABSTRACT UL	18. NUMBER OF PAGES 23	19a. NAME OF RESPONSIBLE PERSON GEORGE W YORK, Lt Col, USAF
a. REPORT UNCLAS	b. ABSTRACT UNCLAS	c. THIS PAGE UNCLAS			19b. TELEPHONE NUMBER <i>(Include area code)</i> +44 (0)20 7514 4354

Project Title

**Solar Wind driven autoregression model for Ionospheric short term Forecast
(SWIF)**

Deliverable: Final report

Authors

Anna Belehaki, Ioanna Tsagouri, Kostas Koutroumbas
National Observatory of Athens, Greece

June 2008

EOARD Award FA8655-07-M-4008

Project manager: George York (george.york@london.af.mil)

Table of contents

List of Figures	3
Introduction and summary of the progress achieved.....	5
1. Development of the upgraded STIM	7
1.1 Improvement of the STIM method	7
1.1.1 Definition of ionospheric storm alert criteria.....	7
1.1.2 Validation of ionospheric storm alert criteria	7
1.1.3 Reformulation of the STIM model expressions.....	14
1.2 Validation of STIM's performance.....	18
2. The development of the new self-consistent forecasting technique	
SWIF.....	23
2.1 The incorporation of TSAR model	23
2.2 The synthesis of SWIF model.....	28
2.3 Evaluation of SWIF performance	31
3. The on-line tool for the operational use of SWIF model.....	37
4. Conclusions and the way ahead	41
References.....	43

List of Figures

Figure 1: The results of the superposed epoch analysis carried out over the time derivative of IMF-B (top panel), the IMF-B itself (second panel), the IMF-Bz component (third panel) and the Dst index (bottom panel) for 30 storm time intervals listed in Table 2. The vertical line denotes the zero time that corresponds to the onset of the IMF disturbance determined by the proposed criteria. The bars in the plot denote standard deviations.

Figure 2: The IMF magnitude, B , its time derivative, the IMF-Bz component, the Dst index and the ionospheric response in both middle-to-low and middle-to-high latitudes over Europe for the storm event of 30 March – 2April, 2001. The vertical lines indicate the identified IMF disturbance onset.

Figure 3: The “averaged” ionospheric response for middle-to-high (top panels) and middle-to-low latitudes (bottom panels) when the LT of the observation point at IMF disturbance onset is determined in a) the morning sector, b) the prenoon sector, c) the afternoon sector and d) the evening sector. The rectangle denotes the onset sector in each case, while the bars in the plot denote standard deviations. The “averaged” variation of the Dst index is also provided for comparison purposes.

Figure 4: The LT dependence of the time delay in ionospheric negative phase occurrence with respect to the IMF disturbance onset for both middle-to-high (top panel) and middle-to-low (bottom panel) latitudes. The dashed line in the bottom panel corresponds to cases when negative storm effects are not anticipated by STIM (daytime hours at middle-to-low latitudes).

Figure 5: The ionospheric response at middle-to-high (a) and middle-to-low (b) latitudes in each local time sector modeled by a 6th degree polynomial function. The vertical line denotes the onset of the ionospheric storm time response.

Figure 6: STIM’s predictions in respect to actual observations for the selected storm time intervals over Chilton (a), Juliusruh (b), Tortosa (c), and Rome (d). The regression line and the corresponding equation in each case are also provided in the plots.

Figure 7: Relative deviations of the observations from the model’s predictions for the selected storm time intervals grouped into four bins depending on the level of the ionospheric activity for four ionospheric stations in absolute values.

Figure 8: The averaged running root mean square error (RMSE) of the observed from modelled values estimated over a 3 hour time window from the beginning to the end of the disturbance for middle-to-high and middle-to-low latitudes.

Figure 9: Ionospheric observations, monthly median estimates and STIM’s predictions for Boulder location during the storm time intervals: 11-13 April, 2001 (top panel) and 3-6 September, 2002 (bottom panel). The relative improvement of STIM’s predictions over climatology during the main storm days is also shown.

Figure 10: The average values of the MSE over each season for quiet intervals using the prediction results of TSAR2 (top), TSNN2 (bottom) for Athens location, for prediction windows 1hr, 3hrs and 6hrs.

Figure 11: The mean absolute relative error estimates for Athens as a function of the prediction step (1-24 hours ahead) for each season.

Figure 12: *The mean absolute relative error values for Athens location and for prediction windows 15min, 1hr, 3hrs and 6hrs calculated over the three phases of each storm (initial, main and recovery) using the prediction results of the two methods TSNN2 (left), and TSAR2 (right).*

Figure 13: *TSAR's predictions in respect to actual observations for the six storm time intervals listed in Table 1 and for various prediction steps: 1h ahead (first panel), 3h ahead (second panel), 6h ahead (third panel) and 24 h ahead (last panel). The results are grouped into three columns, one for each storm day: the pre-storm, the main storm and the post-storm day. The regression line and its equation are also plotted in each case.*

Figure 14: *STIM's predictions in respect to actual observations for the six storm time intervals listed in Table 1. The results are grouped into three columns, following roughly the day-to-day ionospheric storm development. Three days are distinguished: the pre-storm day, the main storm day post-storm day. The regression line is also plotted in each case.*

Figure 15: *The averaged RMSE per storm day over all the events listed in Table 1.*

Figure 16: *Diagram showing the SWIF synthesis.*

Figure 17: *Athens Digisonde ionograms autoscaled with ARTIST4.0 (top) and with ARTIST4.5 (bottom) during fall quiet intervals*

Figure 18: *Athens Digisonde ionograms autoscaled with ARTIST4.0 (top) and with ARTIST4.5 (bottom) during summer quiet intervals*

Figure 19: *Comparison of SWIF and GCAM predictions during the storm events listed in Table 4*

Figure 20: *Scatter plots of e_2 versus e_1 for the time intervals analysed in this part of the analysis. The regression line and its equation are also shown, together with the estimated prediction efficiency, P_{eff} .*

Figure 21: *The storm detection algorithm applied for SWIF on-line implementation, using real-time data from ACE satellite (<http://www.swpc.noaa.gov/ftpdir/lists/ace/>)*

Figure 22: *On-line SWIF implementation results under quiet conditions*

Figure 23: *On-line SWIF implementation results under storm conditions*

Introduction and summary of the progress achieved

In the frames of this project, the end-to-end short-term (up to 24 hours ahead) ionospheric prediction service, SWIF (Solar Wind driven autoregression model for Ionospheric short-term Forecast) is developed and implemented on line.

The new model is based on the critical combination of the TSAR and STIM models into one operational algorithm: Under quiet solar wind conditions, ionospheric forecasts up to 24 hours ahead are derived using the TSAR model. Upon the issuing of an alert, which is based on the real-time analysis of ACE interplanetary magnetic field data, the STIM model is activated with a time delay that depends on the latitude and the local time of the geographic location for which the forecast is required. For the needs of this project, the implementation of SWIF model is applied for Athens location.

The main steps that were followed to develop the new forecasting technique are:

1. The definition of criteria to issue an alert signal based on the on-line analysis of interplanetary magnetic field data from the ACE satellite and the validation of this set of criteria based on historical data analysis (Belehaki et al., 2007a; 2007b).
2. The upgrade of STIM which is the storm-time component of the SWIF model (Belehaki et al., 2007a; 2007b)
3. The evaluation of the performance of the upgraded STIM in comparison to actual observations during storm events and to monthly median conditions (Belehaki et al., 2007b)
4. The synthesis of SWIF which is based on the incorporation of the TSAR model for forecasts under quiet conditions and on the upgraded STIM for calculating ionospheric forecasts upon the issuing of an alert signal.
5. The validation of SWIF model through the evaluation of its performance in comparison to GCAM, which is the most well known model for ionospheric forecasts
6. The on line implementation of the SWIF model for ionospheric predictions over Athens up to 24 hours ahead, which is driven by real-time streaming ACE data.

The on-line implemented SWIF model with the results of short term forecasts over Athens up to 24 hours ahead, are accessible through the web address <http://195.251.203.13/ACE/CurrentACE/CurrentACE.html>.

An on-line documentation is available for user guidance.

Presentations in conferences and international meetings:

1. “Ionospheric forecasts over Europe driven by IMF conditions”, Tsagouri I. and A. Belehaki, 4th *European Space Weather Week*, 5-9 November 2007, Brussels.
2. “Space Weather and Ionosphere”, Belehaki A., in *International School of Space Science*, L’Aquila, Italy, 7-11 April 2008.
3. “Solar wind driven autoregression model for short term ionospheric forecast” Tsagouri I., K. Koutroumbas and A. Belehaki, *European Geosciences Union General Assembly*, 14-18 April 2008, Vienna, Austria (Invited paper)
4. “Solar wind driven autoregression model for short term ionospheric forecast” Tsagouri I., K. Koutroumbas and A. Belehaki, *Ionospheric Effects Symposium*, 12-16 May 2008, Alexandria, VA, USA (Supported by EOARD WOS Grant FA8655-08-1-2041)
5. “A new ionospheric forecast model assimilating solar wind data and ground based ionosonde observations”, I. Tsagouri, K. Koutroumbas and A. Belehaki, 12th *International Symposium on Equatorial Aeronomy (ISEA)*, 19-23 May 2008, Crete, Greece
6. “From DIAS to EURIPOS: the European Research Network of Ionospheric and Plasmaspheric Observation Systems”, *Environmental Monitoring and Geohazards in the Mediterranean*, 6 June 2008, Crete, Greece

Papers:

1. Solar wind driven autoregression model for short term ionospheric forecast, Tsagouri I., K. Koutroumbas and A. Belehaki, *Proceedings of the Ionospheric Effects Symposium*, 2008, Alexandria, VA, USA
2. An upgrade of the solar wind driven empirical model for the middle latitude ionospheric storm time response, Tsagouri I. and A. Belehaki, *Journal of Atmospheric and Solar Terrestrial Physics*, 2008 (Submitted)
3. “A new ionospheric forecast model assimilating solar wind data and ground based ionosonde observations”, I. Tsagouri, K. Koutroumbas and A. Belehaki, *CD Proceedings of the 12th International Symposium on Equatorial Aeronomy (ISEA)*, 19-23 May 2008, Crete, Greece

1. Development of the upgraded STIM

1.1 Improvement of the STIM method

The STIM method was introduced by Tsagouri and Belehaki (2006) as a storm time ionospheric model triggered by solar wind conditions. In its first version, STIM includes a rather qualitative approach for the determination of the alert conditions, while the latitudinal dependence of the ionospheric storm time response is not anticipated. For the needs of this project that aims on the development of an operational ionospheric forecasting model applicable at middle latitudes, it was necessary to define accurate ionospheric storm alert criteria, to reformulate STIM model expressions in order to include also the latitudinal dependence and finally to validate STIM.

1.1.1 Definition of ionospheric storm alert criteria

Based on past developments (Belehaki and Tsagouri, 2002; Tsagouri and Belehaki, 2006) and on the existing literature (Gonzalez and Tsurutani, 1987; Tsurutani and Gonzalez, 1995; Gonzalez et al., 1999; 2001), a set of conditions have been identified that should be fulfilled in order to issue an alert for forthcoming geomagnetic storm with impact on the ionosphere:

- i. The IMF-B should record either a rapid increase denoted by time derivative values greater than 3.8 nT/h or absolute values greater than 13 nT.
- ii. The IMF-Bz component should be southward directed either simultaneously or a few hours later. In particular, based on preliminary analysis, intense storm conditions ($B_z < -10$ nT for at least three hours) are verified maximum 6 hours later.
- iii. Each event ends when Bz is turned northward ($B_z > -1$ nT).

The on-line analysis of IMF data from the ACE spacecraft, allows the real-time identification of alert conditions.

1.1.2 Validation of ionospheric storm alert criteria

The validation was based on the analysis of hourly IMF-Bz component and IMF-B data in GSM coordinate system from MAG experiment onboard ACE spacecraft, of hourly Dst index data and hourly values of the ionospheric critical frequency foF2 obtained from eight ionospheric stations located in the middle latitude European region for the time interval 1998 – 2005. The list of the ionospheric stations is given in Table 1. The Dst index was used for the identification of storm occurrence. The ionospheric response over Europe was determined in comparison to monthly median conditions and the ratio foF2obs/foF2median was used as ionospheric disturbance index. To include the latitudinal dependence of the ionospheric response, we identified two latitude zones, the middle-to-high latitudes zone for latitudes greater than 45° N (the case of Chilton and Juliusruh), and the middle-to-low latitudes zone for latitudes from 30° to 45° N (the case of Athens, Rome, San Vito, Sofia, El Arenosillo and Tortosa).

Table 1: List of ionospheric stations

Station	Geographic Longitude (° E)	Geographic Latitude (° N)
Athens	23.8	38.1
Chilton	358.7	51.6
El Arenosillo	353.3	37.1
Juliusruh	13.4	54.6
Rome	12.5	41.8
San Vito	17.8	40.6
Sofia	23.4	42.7
Tortosa	0.3	40.4

a) Validation based on IMF and Dst index data : During the 7 years (1998-2005) of data analyzed for validation purposes, 107 alert signals have been determined, using the set of criteria summarized in section 1.1.1. These alerts have been cross checked with actual events of geomagnetic storm activity identified by the Dst index. The results show that 76 alerts were related to 57 intense ($-200 \text{ nT} \leq \text{Dst} < -100 \text{ nT}$) or big ($\text{Dst} < -200 \text{ nT}$) storms, while for 15 of these storms more than one alert was determined. A case-by-case study of these events showed a one-to-one relationship between the received alerts and storm intensifications occurred in success either during the storm main phase (for storms with multiple onsets) or during the storm recovery phase (for successive storm events). Here it is important to note that the 57 predicted storm time intervals corresponds to the 84% of the total number of intense or big storm events that occurred in the examined period, which is 68. Moreover, 30 of the received alerts corresponds to moderate ($-100 \text{ nT} < \text{Dst} < -50 \text{ nT}$) storm activity, while only one seems to be a clear false alarm since both the geomagnetic and ionospheric activity that followed this alert signal remained at really low level.

To summarize the phenomenology of the interplanetary magnetic field conditions causing intense magnetic storms, we analyzed 30 storm events (see the list of intervals in Table 2) that are mainly storm events with well defined phases. In this sample, 14 storm events occurred around solar maximum (1999-2001), 6 near solar minimum (2004 – 2005), and 10 events at the intermediate phases. Concerning the storm intensity, 19 are intense storms ($-200 \leq \text{Dst} < -100 \text{ nT}$) and 11 are big storms.

Table 2: List of storm events used for the upgrade of STIM

Time Interval	<i>min</i> Dst (nT)
9-12 March 1998	-116
25-27 June 1998	-101
26-28 August 1998	-155
24-26 September 1998	-207
12-17 November 1998	-131
12-17 January 1999	-112
17-21 February 1999	-123
22-24 September 1999	-173
21-24 October 1999	-237

6-8 April 2000	-288
15-17 July 2000	-301
17-19 September 2000	-193
6-10 November 2000	-159
30 March – 1 April 2001	-387
17-19 April 2001	-114
17-18 August 2001	-105
27-30 October 2001	-157
5-8 November 2001	-292
24-27 November 2001	-221
11-13 May 2002	-110
7-9 September 2002	-181
29-31 May 2003	-144
17-20 August 2003	-148
19-22 November 2003	-422
21-23 January 2004	-149
6-9 November 2004	-373
9-11 November 2004	-289
14-18 May 2005	-263
12-14 June 2005	-106
31 Aug–1 Sep 2005	-131

The average interplanetary magnetic field response has been extracted with superposed epoch analysis and the results are presented in Figure 1. The zero time of the superposed epoch analysis, denoted by the vertical line, corresponds to the IMF disturbance onset as it is determined by the introduced criteria.

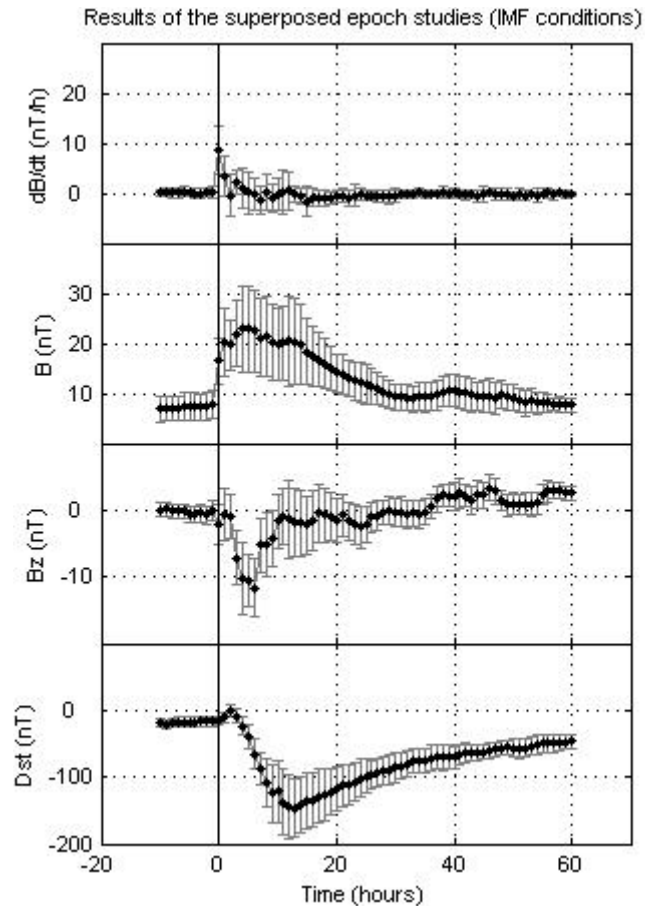


Figure 1: *The results of the superposed epoch analysis carried out over the time derivative of IMF-B (top panel), the IMF-B itself (second panel), the IMF-Bz component (third panel) and the Dst index (bottom panel) for 30 storm time intervals listed in Table 2. The vertical line denotes the zero time that corresponds to the onset of the IMF disturbance determined by the proposed criteria. The bars in the plot denote standard deviations.*

From the overall picture revealed in Figure 1, the first indication of forthcoming disturbances comes indeed from the increase in the magnitude of the IMF, while B gets values significantly greater than 8 nT and Bz is turned southward three hours later. The storm main phase onset denoted by the decrease in Dst index follows the Bz southward turning a couple of hours later and the ionospheric response follows with a certain time delay, which is strongly depended on the LT of the observation point, as it is demonstrated in the following section.

b) Validation based on ionospheric data: As a first approach we show the ionospheric response together with the temporal evolution of the IMF characteristics during a storm event occurred on 31 March to 1 April 2001 (Figure 2). For this time interval, two alert signals are received according to the B, dB/dt and Bz criteria and they are indicated with the vertical lines: the first on 31 March at 0000 UT and the second on 31 March at 1200 UT. These alerts are consistent with two successive reductions of the Dst index. The prolonged ionospheric response at middle latitudes in both latitudinal zones is in consistency with Prölss (1993) phenomenological model:

negative storm effects are recorded by all stations for two successive days as a response to two individual storm events. The effect is clearer at middle-to-low latitudes where the ionospheric disturbance that followed the first storm event has been totally recovered before the second one. This first confirms the validity of the latitudinal distinction of the middle latitude ionosphere into two zones and then provides evidence for the efficiency of the proposed method in anticipating multiple or successive storm disturbances.

For statistical validation purposes we present the average ionospheric response in correspondence to the storm alerts, for the 30 storm events listed in Table 2. Concerning the seasonal distribution, the storm events could be sorted by three seasons (Fuller-Rowell et al., 2000): 6 storm events occurred during summer months (May, June, July), 9 during winter months (November, December, January), and 15 during equinox time. This distribution supports the validity of our results for all possible conditions.

The results of the superposed epoch analysis are presented in Figure 3. Taking into account the local time dependence of the ionospheric response, the ionospheric observations were further organized in eight groups based on the latitude and the local time (LT) of the observation point at zero time. Four LT sectors are defined as follows: evening (1800-0000 in LT), morning (0000 – 0600 in LT), prenoon (0600 – 1200 in LT) and afternoon (1200-1800 in LT). The zero time falls into the denoted rectangular in each case (Figure 3).

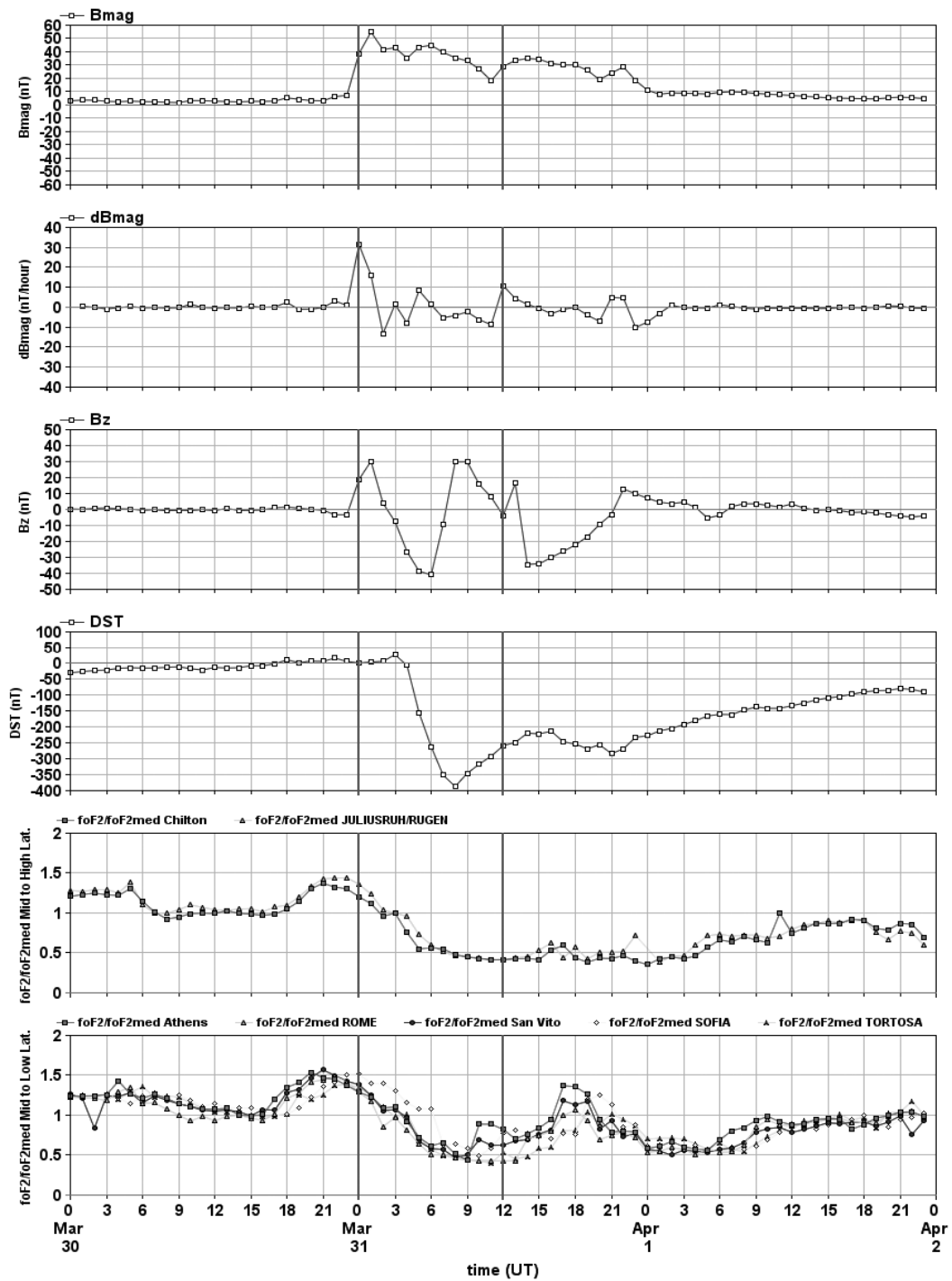


Figure 2: The IMF magnitude, B , its time derivative, the IMF- B_z component, the Dst index and the ionospheric response in both middle-to-low and middle-to-high latitudes over Europe for the storm event of 30 March – 2April, 2001. The vertical lines indicate the identified IMF disturbance onsets.

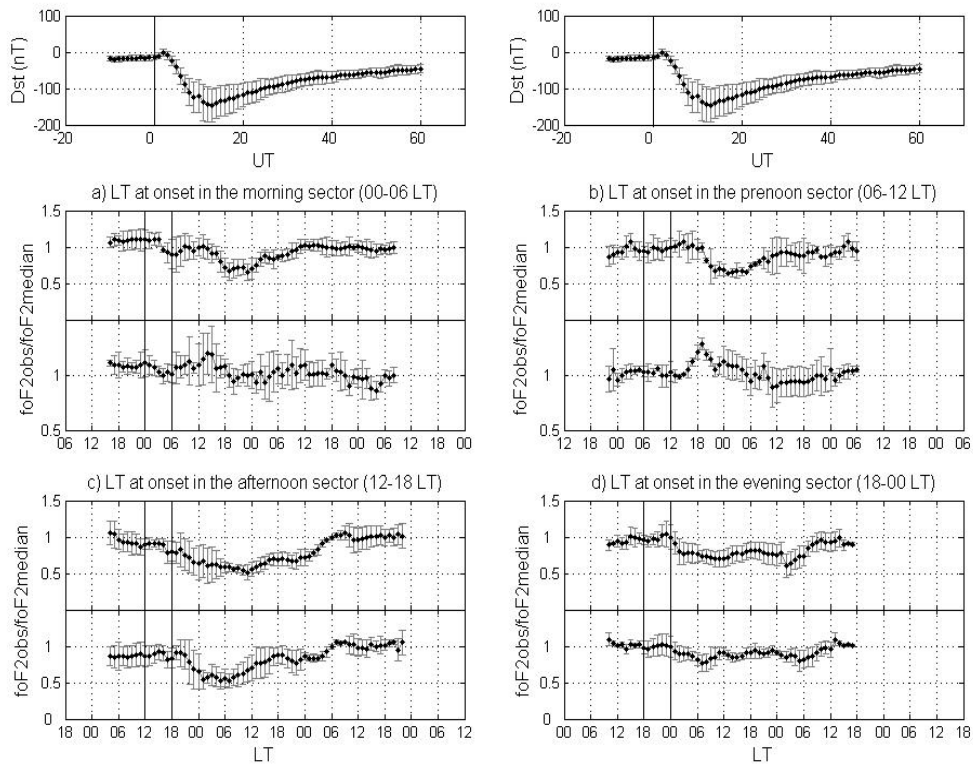


Figure 3: The “averaged” ionospheric response for middle-to-high (top panels) and middle-to-low latitudes (bottom panels) when the LT of the observation point at IMF disturbance onset is determined in a) the morning sector, b) the prenoon sector, c) the afternoon sector and d) the evening sector. The rectangle denotes the onset sector in each case, while the bars in the plot denote standard deviations. The “averaged” variation of the Dst index is also provided for comparison purposes.

Concerning the ionospheric response, significant positive storm effects (greater than 20% in respect to monthly median values) are systematically observed only at middle-to-low latitudes most probably because higher latitudes are covered by the generated neutral composition disturbance zone as a prompt response to the storm activity. The positive phase is detected during daytime hours, about a few hours later than zero time and when the observation point is located in the morning and prenoon sectors at the disturbance onset. The positive phase penetrates to the evening sector, which is in agreement with the Fuller-Rowell et al. (1994) scenario. Negative phases of the ionospheric response are systematically observed in middle-to-high latitudes independently on the LT of the observation point and in the middle-to-low latitudes in the nighttime hours. In all cases, the negative phase is first detected in the evening sector while it is expanded in the daytime hours as the storm develops and recovers. The response is very fast when the ionospheric stations are located in the evening (18:00 – 02:00 LT) sector. This is consistent with the generation of the neutral gas composition disturbance zone in the post midnight sector and its expansion towards middle latitudes during the storm period. Then, the maximum in the time delay between the onset and the appearance of the negative ionospheric storm phase at middle latitudes, is recorded when the LT time of the observation point is around

dawn, since ionospheric stations should rotate into the evening sector in order to “meet” the neutral composition disturbance zone.

Summarizing, it was demonstrated that the ionospheric storm time disturbances follow with a certain time delay the onset in IMF disturbances as it is determined by the introduced criteria and then that they are consistent with Prölss (1993) and Fuller-Rowell et al. (1994;1996) phenomenological scenario, verifying the validity of the introduced criteria for ionospheric forecasting purposes.

1.1.3 Reformulation of the STIM model expressions

The purpose of the reformulation is to include the latitudinal dependence of the ionospheric response and it is based on the analysis of the observations during a significant number of storm events.

First, the time delay of the ionospheric disturbance onset in respect to the IMF disturbance onset was estimated in all the events under study. Only ionospheric disturbances greater than 20% were taken into account in our analysis. For positive storm effects the time delay was estimated at 3 hours independent on the LT of the observation point, but only for daytime hours at middle-to-low latitudes. Concerning the onset of the negative storm phase the results are presented in Figure 4 for both latitudinal zones versus the LT of the observation point. The LT effect of the ionospheric response is well reflected in the obtained curves. The evening and post-midnight ionosphere responds faster (in about two or three hours) to IMF disturbances, while the maximum delay (about 12 hours) is recorded when the observation point is located around dawn at the IMF disturbance onset.

The ionospheric response was formulated in each LT sector and for each latitudinal zone. Fig. 5 shows the superposed epoch analysis results of the ionospheric response in each LT sector and for middle-to-high (a) and middle- to-low latitudes (b) respectively. Now the zero time corresponds to the onset of the ionospheric storm time response. The best-fit curve to the $y=foF2_{obs}/foF2_{med}$ variation is a polynomial of 6th degree and the coefficients are provided in Table 3. This equation serves as the modeling expression for the ionospheric response in each LT sector.

In general, negative effects are anticipated as a global response in middle-to-high latitudes while at the lower latitudes daytime positive effects are included in the model's predictions. According to the models predictions, the duration of ionosphere storm time response depends strongly on the LT and the latitude of the observation point, lasting from 10 (for positive storm effects at middle-to-low latitudes) up to 40 hours (for negative storm effects at middle-to-high latitudes triggered in the afternoon sector). Taken into account the corresponding time delay in the ionospheric storm onset, which is 3 hours for positive storm effects and about 5 hours for negative storm effects triggered in the afternoon sector (Figure 5), STIM's ionospheric predictions are provided from 13 up to 45 hours ahead.

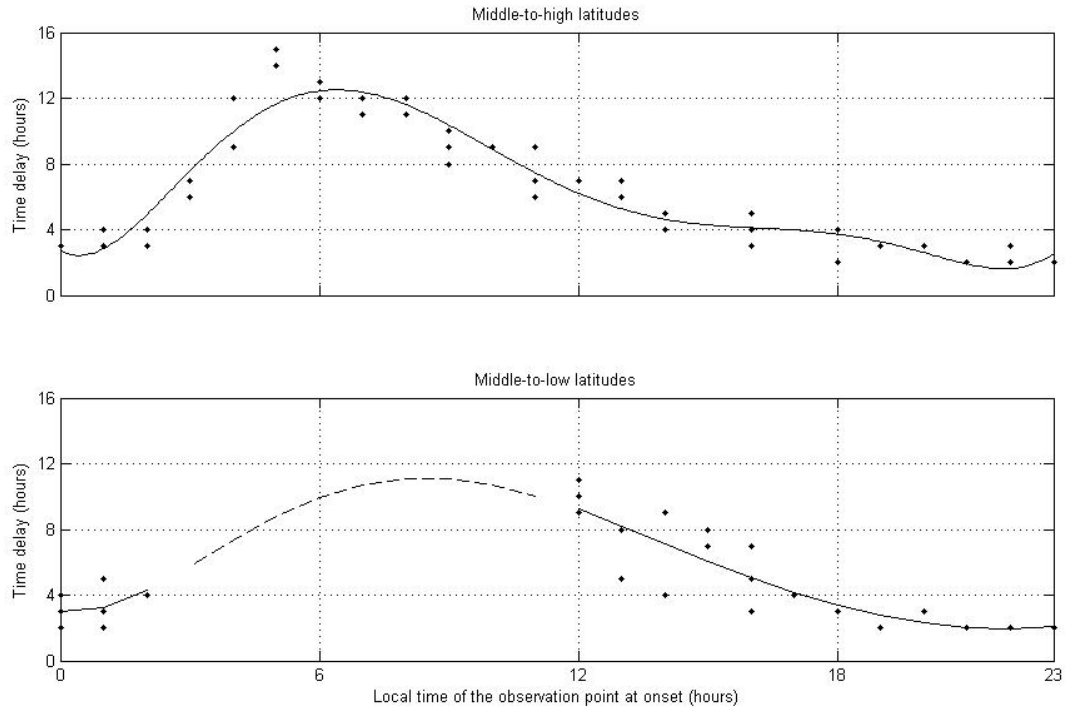


Figure 4: The LT dependence of the time delay in ionospheric negative phase occurrence with respect to the IMF disturbance onset for both middle-to-high (top panel) and middle-to-low (bottom panel) latitudes. The dashed line in the bottom panel corresponds to cases when negative storm effects are not anticipated by STIM (daytime hours at middle-to-low latitudes).

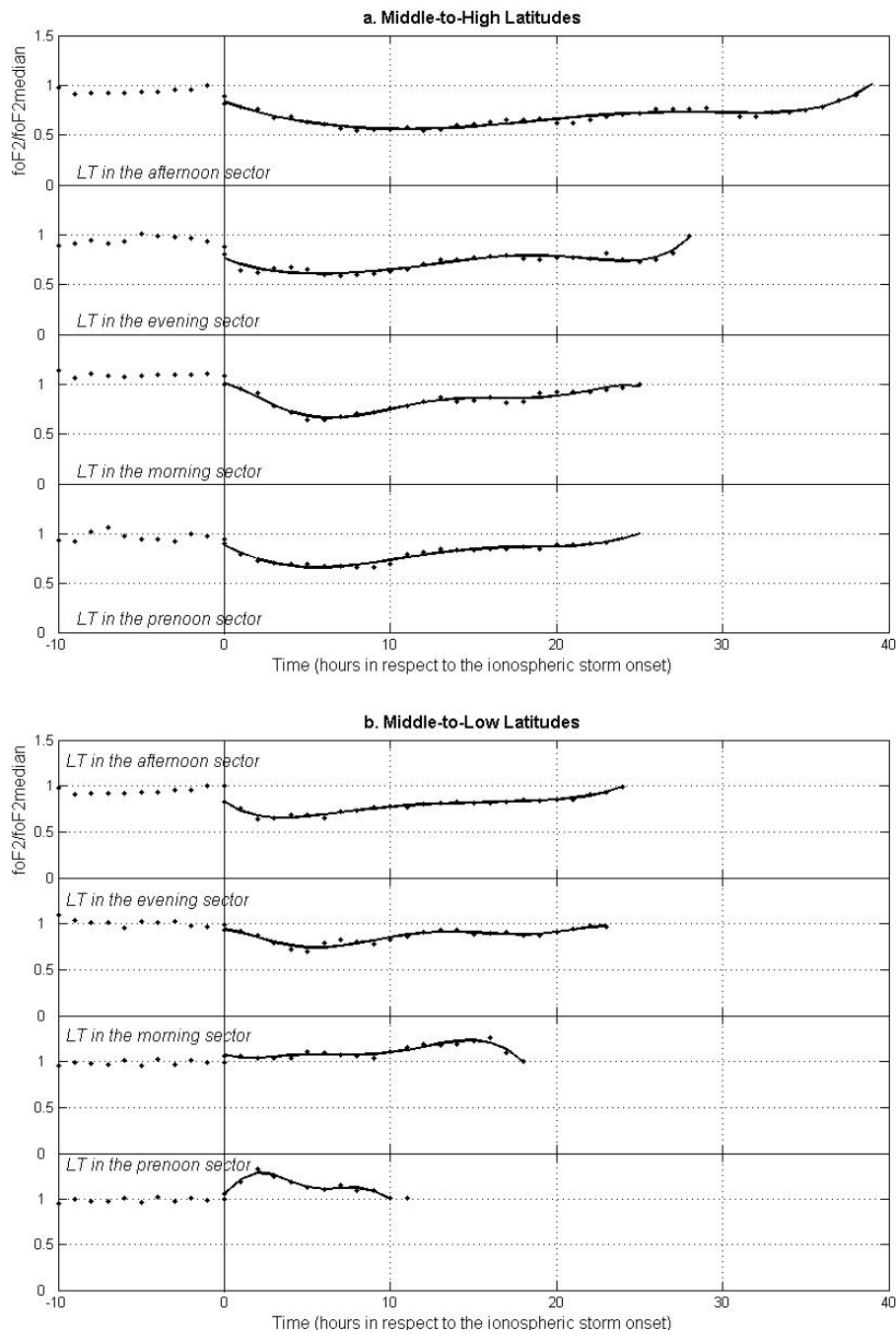


Figure 5: The ionospheric response at middle-to-high (a) and middle-to-low (b) latitudes in each local time sector modeled by a 6th degree polynomial function. The vertical line denotes the onset of the ionospheric storm time response.

Table 3: The coefficients of the polynomial function $y=A_6x^6 + A_5x^5 + A_4x^4 + A_3x^3 + A_2x^2 + A_1x + A_0$ that best fit to the ionospheric storm time response in each case.

Middle-to-high latitudes

LT sector	A_6	A_5	A_4	A_3	A_2	A_1	A_0
Afternoon	$50 \cdot 10^{-10}$	$-42 \cdot 10^{-8}$	$13 \cdot 10^{-6}$	$-23 \cdot 10^{-5}$	$47 \cdot 10^{-4}$	$-60 \cdot 10^{-3}$	$83 \cdot 10^{-2}$
Evening	$53 \cdot 10^{-9}$	$-36 \cdot 10^{-7}$	$93 \cdot 10^{-6}$	$-13 \cdot 10^{-4}$	$13 \cdot 10^{-3}$	$-70 \cdot 10^{-3}$	$76 \cdot 10^{-2}$
Morning	$-26 \cdot 10^{-8}$	$20 \cdot 10^{-6}$	$-55 \cdot 10^{-5}$	$66 \cdot 10^{-4}$	$-27 \cdot 10^{-3}$	$-38 \cdot 10^{-3}$	$100 \cdot 10^{-2}$
Prenoon	$-18 \cdot 10^{-9}$	$18 \cdot 10^{-7}$	$-54 \cdot 10^{-6}$	$33 \cdot 10^{-5}$	$73 \cdot 10^{-4}$	$-84 \cdot 10^{-3}$	$88 \cdot 10^{-2}$

Middle-to-low latitudes

LT sector	A_6	A_5	A_4	A_3	A_2	A_1	A_0
Afternoon	$62 \cdot 10^{-9}$	$-52 \cdot 10^{-7}$	$18 \cdot 10^{-5}$	$-34 \cdot 10^{-4}$	$33 \cdot 10^{-3}$	$-13 \cdot 10^{-2}$	$83 \cdot 10^{-2}$
Evening	$-32 \cdot 10^{-8}$	$23 \cdot 10^{-6}$	$-61 \cdot 10^{-5}$	$69 \cdot 10^{-4}$	$-28 \cdot 10^{-3}$	$-84 \cdot 10^{-4}$	$94 \cdot 10^{-2}$
Morning	$50 \cdot 10^{-8}$	$-33 \cdot 10^{-6}$	$78 \cdot 10^{-5}$	$-82 \cdot 10^{-4}$	$39 \cdot 10^{-3}$	$-69 \cdot 10^{-3}$	$110 \cdot 10^{-2}$
Prenoon	$29 \cdot 10^{-6}$	$-89 \cdot 10^{-5}$	$97 \cdot 10^{-4}$	$-40 \cdot 10^{-3}$	$22 \cdot 10^{-3}$	$17 \cdot 10^{-2}$	$110 \cdot 10^{-2}$

1.2 Validation of STIM's performance

All available ionospheric observations from four European stations, Chilton and Juliusruh from the middle-to-high latitudinal zone and Tortosa and Rome from the middle-to-low latitudinal zone obtained during the time intervals listed in Table 4 were used for the validation of the proposed method.

Table 4: List of the storm events used for validation tests

Time Interval	min Dst (nT)	Determined onsets
1-8 May 1998	-205	3
5-8 August 1998	-138	1
18-22 October 1998	-112	1
6-11 November 1998	-149	2
	-142	
11-13 February 2000	-133	1
23-26 May 2000	-147	1
10-14 August 2000	-106	2
	-235	
2-8 October 2000	-182	2
	-143	
12-17 October 2000	-107	2
28-31 October 2000	-127	1
19-22 March, 2001	-149	1
11-13 April 2001	-271	1
21-25 April 2001	-102	1
30 Sep - 6 Oct 2001	-166	1
21-25 October 2001	-187	2
	-160	
17-23 April, 2002	-127	4
	-149	
3-6 September 2002	-109	1
30 Sep – 2 Oct 2002	-162	1
16-21 June 2003	-141	1
10-13 July 2003	-105	1
28 Oct – 1 Nov 2003	-353	2
	-383	
10-12 February 2004	-109	1
22-30 July 2004	-101	3
	-148	
	-197	
30 Aug. – 1 Sept. 2004	-126	1
17-20 January 2005	-121	1
7-10 May 2005	-127	1
29-31 May 2005	-138	1

The time intervals correspond to intense or big storm events. The onset of the disturbance was determined from IMF conditions using the proposed criteria and the corresponding ionospheric response was modelled by STIM's estimations. It is worthy to note that for 9 of these events more than one onsets were determined (the number of the determined onsets in each case are given in the last column of Table 4) and that each of them was individually included in our analysis. The results are

summarized in Figure 6 where the model's predictions are compared to the actual observations, showing a statistically significant correlation for all stations.

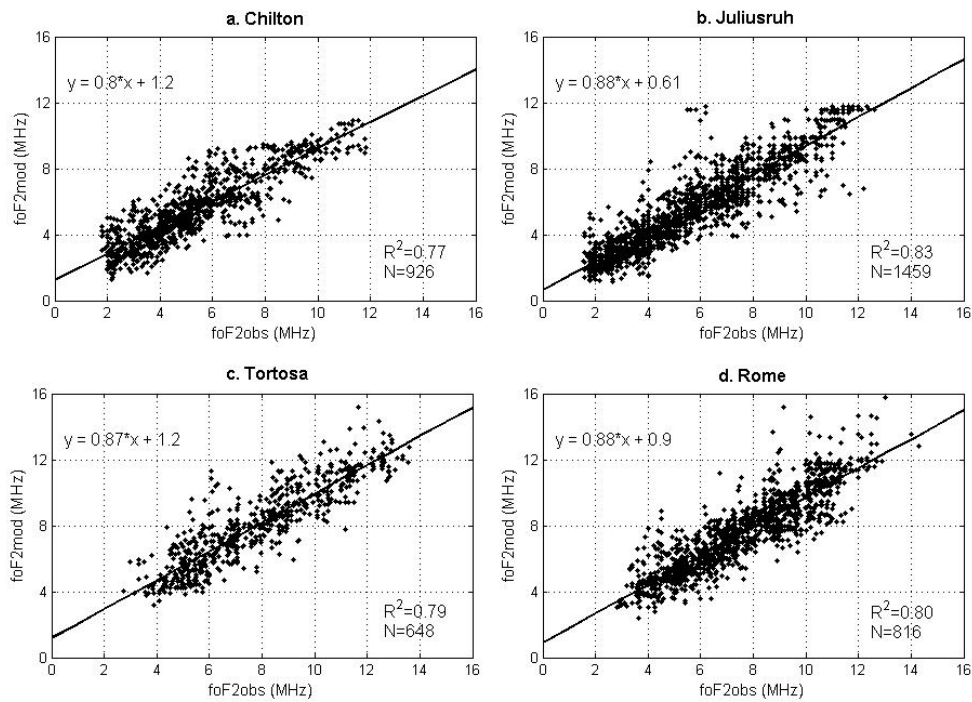


Figure 6: *STIM's predictions in respect to actual observations for the selected storm time intervals over Chilton (a), Juliusruh (b), Tortosa (c), and Rome (d). The regression line and the corresponding equation in each case are also provided in the plots.*

To evaluate the model's performance in respect to the level of the ionospheric activity, the relative deviation of the observed values from the model's predictions was estimated in respect to the relative deviation of the observed from monthly median estimations. Only negative disturbances were considered here, since they are the global feature of the ionospheric response. The results were grouped into four bins depending on the level of the ionospheric activity and are given in Figure 7 for all ionospheric stations in absolute values, while all original figures comes with negative signs. As a first comment, the negative sign of the relative deviation of the observed values from the model's predictions in all cases in conjunction to the occurrence of negative storm phase shows that the model's prediction seems to underestimate the ionospheric disturbances. The prediction error increases with the level of the ionospheric activity. It is smaller than 10% for moderate-to-low (20-30%) ionospheric activity and fair (up to 16%) for moderate ionospheric activity (30-40%). The prediction error is increased up to 21% for intense ionospheric activity (40-50%) and up to 32% for very intense (greater than 50 %) ionospheric disturbances for middle-to-high latitudes.

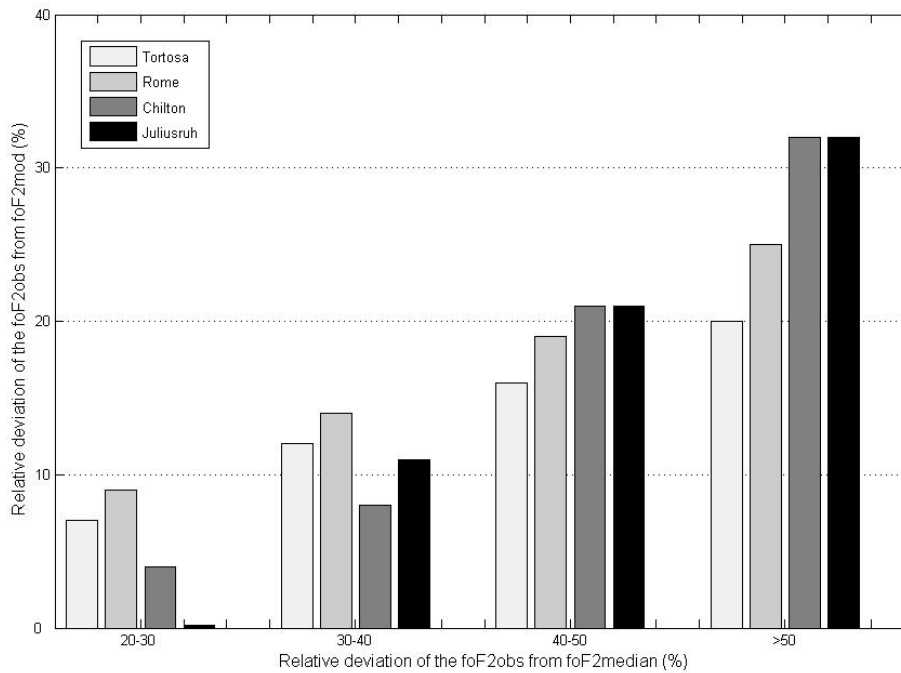


Figure 7: *Relative deviations of the observations from the model’s predictions for the selected storm time intervals grouped into four bins depending on the level of the ionospheric activity for four ionospheric stations in absolute values.*

The model’s performance was next investigated in respect to the temporal evolution of the ionospheric storm time disturbance. For this purpose the averaged running root mean square error (RMSE) of the observed from modelled values was estimated over a 3 hour time window from the beginning to the end of the disturbance. Once again only negative disturbances were considered. The results are presented in Figure 8 for both middle-to-high and middle-to-low latitudes. At middle-to-high latitudes the RMSE is small during the whole of the disturbance since it hardly exceeds 1 MHz. For lower latitudes, the error appears small (smaller than 1.5 MHz) at the beginning of the disturbance and during the first 10 hours as well as at the last 5 hours, indicating that the model captures successfully the onset and the recovery of the disturbance. The error increased to about 2.5 MHz about 15 hours after the onset. This in our opinion indicate that the model, although follow the disturbance, it doesn’t yield its intensity.

A widely used way to demonstrate the merits of the method is to compare its predictions with the monthly median predictions (Mikhailov et al., 2007). Here, the relative improvement over climatology was estimated by the formula: % improvement = ((RMSE(monthly median)-RMSE(model)/RMSE(monthly median))x100 (Araujo-Pradere and Fuller-Rowell, 2002) for each storm day. The results were grouped for each season and are given in Table 5. The best performance (55% improvement over climatology) is recorded at the middle-to-high latitudes during equinox time, while the poorer (27%) is recorded at middle-to-low latitudes during winter. The averaged (over all stations) improvement over climatology during equinox is 44%, while during summer and winter months is estimated at 36% and 30%, respectively. Therefore, concerning the seasonal dependence of STIM’s performance, one can argue that the model’s predictions stand better for equinox time and poorer during winter time. A better performance for the higher latitudes is also verified for all seasons. This trend is

also reflected in the averaged (over all seasons) relative improvement, which is estimated to be 43% for the higher latitudes, and 29% for lower latitudes. This results in an overall improvement of 36% over climatology by using STIM's methodology.

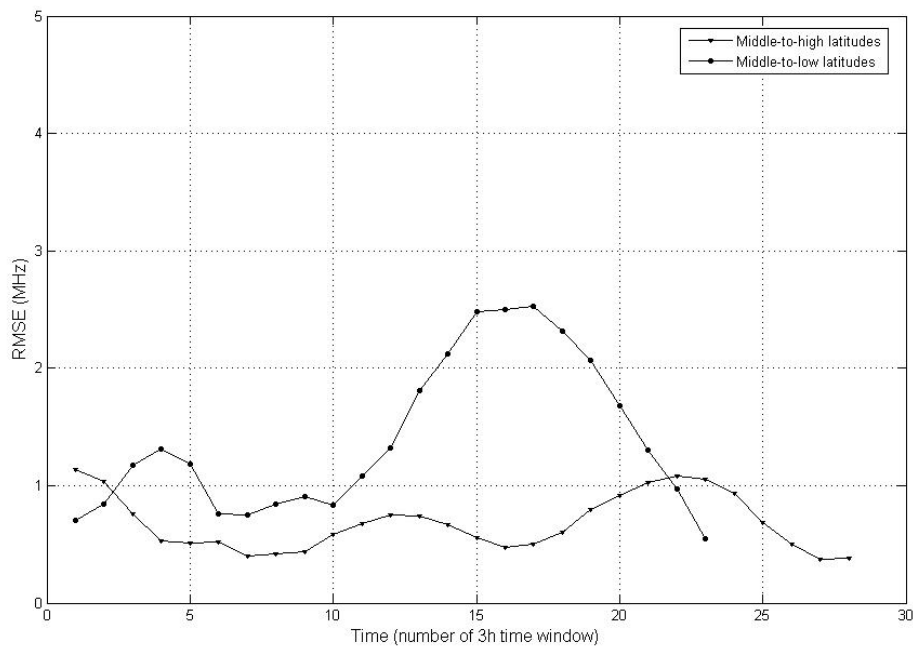


Figure 8: The averaged running root mean square error (RMSE) of the observed from modelled values estimated over a 3 hour time window from the beginning to the end of the disturbance for middle-to-high and middle-to-low latitudes.

STIM's performance was extensively evaluated here for the European region, but without harm of its generalized application. STIM's is designed to provide ionospheric forecasts at any middle latitude ionospheric location based on the LT of the observation point at the IMF disturbance onset. As an example, STIM's predictions for Boulder location during two storm time intervals (11-13 April, 2001 and 3-6 September 2002) are presented in Figure 9 together with actual observations and monthly median estimates. The relative improvement of STIM's predictions over climatology during the main storm days is also shown in the figure.

Table 5: The relative improvement of STIM's predictions over climatology grouped for three seasons

Season	Test station	% improvement
<i>Summer</i>	Chilton (N=8)	41%
	Juliusruh (N= 15)	44%
	Tortosa (N=5)	33%
	Rome (N=5)	27%
<i>Equinox</i>	Chilton (N=14)	55%
	Juliusruh (N=25)	53%
	Tortosa (N=9)	35%
	Rome (N=9)	30%
<i>Winter</i>	Chilton (N=6)	32%
	Juliusruh (N=5)	33%
	Tortosa (N=3)	30%
	Rome (N=3)	23%

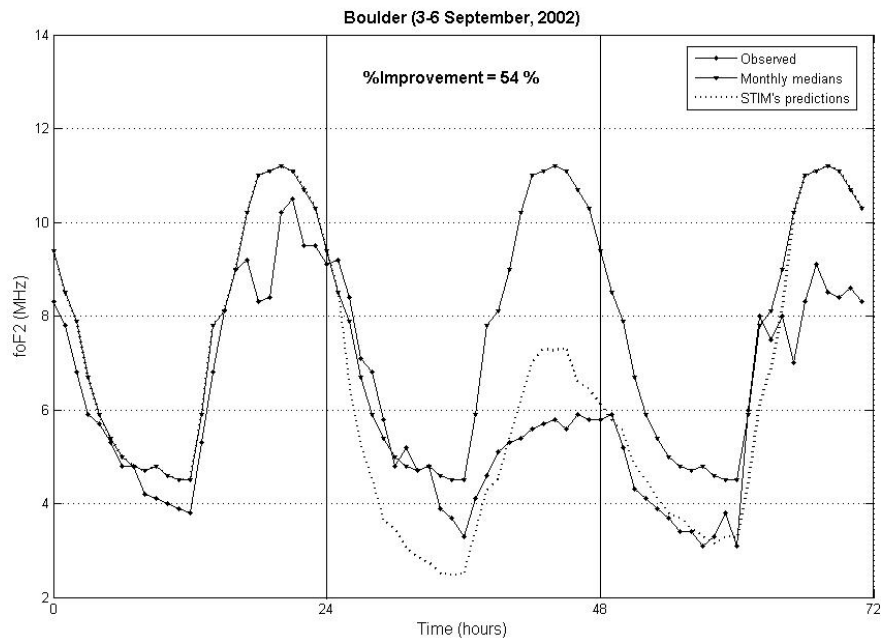
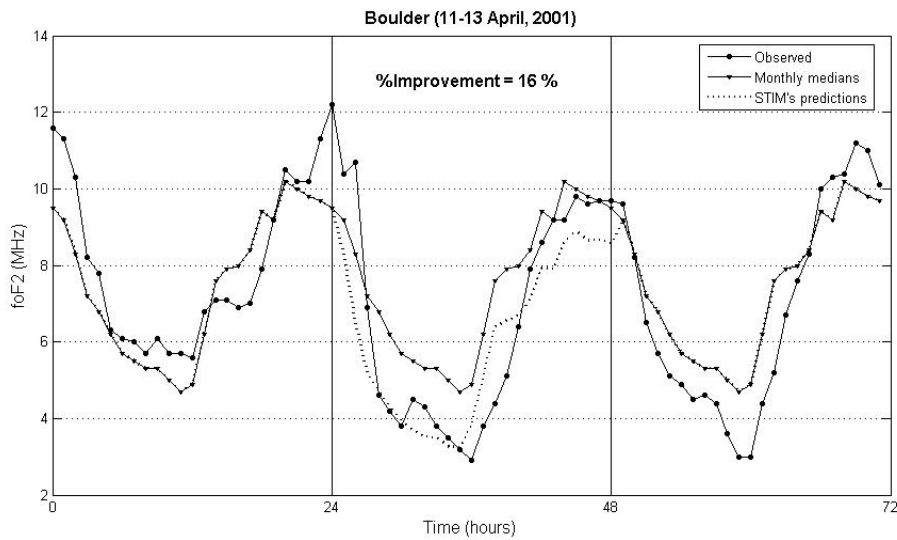


Figure 9: Ionospheric observations, monthly median estimates and STIM's predictions for Boulder location during the storm time intervals: 11-13 April, 2001 (top panel) and 3-6 September, 2002 (bottom panel). The relative improvement of STIM's predictions over climatology during the main storm days is also shown.

2. The development of the new self-consistent forecasting technique SWIF

2.1 The incorporation of TSAR model

The TSAR model is an autoregressive forecasting technique, introduced by Koutroumbas et al. (2008) to forecast the foF2 over specific stations locations. The problem considered is the estimation of foF2 characteristic s steps ahead, based on its current as well as its previous M values, using autoregressive (AR) modeling. Focusing on a specific value of s at the beginning of a calendar month, the data of the previous calendar month are used to estimate the AR model that will be used for the estimation of foF2 for the current calendar month. Various AR models are tested on the above data of the previous calendar month and the best one (according to the mean square error criterion) is adopted. More precisely, taking into account that the sampling rate is 15 min, we would like to have estimates of the foF2 after 15mins ($s=1$), 1hour ($s=4$), 2hours ($s=8$),..., 24hours ($s=96$). Thus, we need to estimate 25 AR models denoted by AR_0 (15mins), AR_1 (1hour), AR_2 (2hours),..., AR_{24} (24hours). Based on the systematic variations of the foF2 value, it has been decided to re-estimate the 25 AR models at the beginning of every calendar month, by taking into account the measurements of the previous calendar month. Note that after its estimation, each AR_i is applied every time a new observation becomes available (in our case every 15mins).

a) Evaluation of Time Series AutoRegressive (TSAR) model

In order to incorporate STIM's triggering and formulation output into the autoregressive algorithm (TSAR), it was first necessary to evaluate the performance of TSAR method. Validation tests through comparisons with other modeling techniques of the same philosophy (e.g. neural network based methods) were carried out and this analysis revealed points of weakness in TSAR's predictions.

The performance of TSAR was compared with predictions obtained using a similar method that, instead of AR models, it uses feed forward neural networks (FNNs) with a single hidden layer, called TSNN (**T**ime **S**eries **N**eural **N**etwork) (Koutroumbas and Belehaki, 2005). The TSNN uses two months of data for training and testing (denoted for this reason as TSNN2 in the next figures) and for reasons of thoroughness, the TSAR2 method (TSAR using 2 month data) was considered in our comparisons. Both TSAR and TSNN methods share the same general philosophy in the sense that each one of them picks the best model (AR and FNN, respectively), among a set of available models. Besides their similarities, TSAR and TSNN differ significantly in the modelling approach: TSAR adopts linear models for the prediction of the absolute foF2 values, while TSNN uses non linear models for the same reason.

The method predictions were evaluated during several geomagnetically quiet time intervals. The average values of the MSE over each season are presented in Figure 10 for Athens location. It is very interesting to note the significant difference comparing the performance of NN and AR models. In the case of AR the MSE doesn't exceed the 1 MHz, while the NN model gives a MSE larger than 4 MHz. Concerning the seasonal

dependence of the methods' performance, the AR models present a consistent pattern with maximum in the MSE during the summer and minimum in winter. This indicates probably a dependence of the model prediction on the automatic scaling performance which during summer presents the maximum error due to frequent sporadic E layer or spread F occurrence, which is very intense over Athens. The seasonal pattern of the MSE obtained using the TSNN method presents noticeable differences, with a minimum in winter but only for prediction horizon greater than 3 hrs.

To explore the reliability of TSAR predictions in ionospheric forecasting from 1 to 24 hours ahead, the mean absolute relative error as a function of the prediction time horizon is shown in Figure 11. The relative error gets relatively small values (4 – 6 %) for predictions 15 min ahead and reaches a maximum value of about 14% for predictions 4 or 5 hours ahead, which in general is maintained and in some cases is decreased for predictions up to 24 hours ahead. This pattern indicates that TSAR method provide statistically reliable ionospheric predictions up to 24 hours ahead and could be considered as robust forecasting technique for the middle latitude ionosphere.

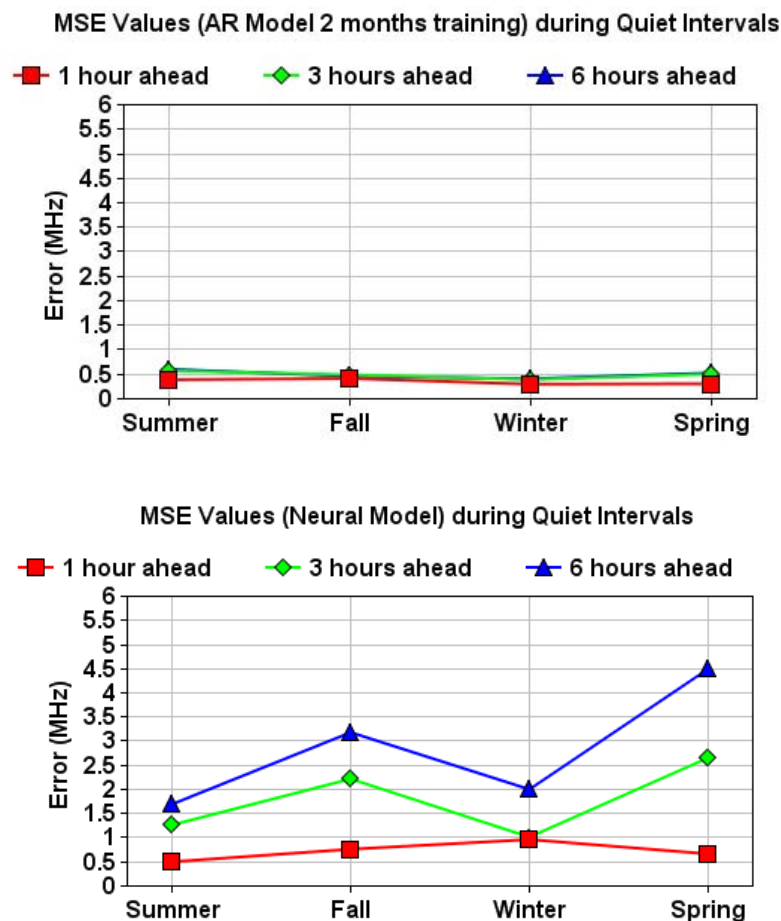


Figure 10: The average values of the MSE over each season for quiet intervals using the prediction results of TSAR2 (top), TSNN2 (bottom) for Athens location, for prediction windows 1hr, 3hrs and 6hrs.

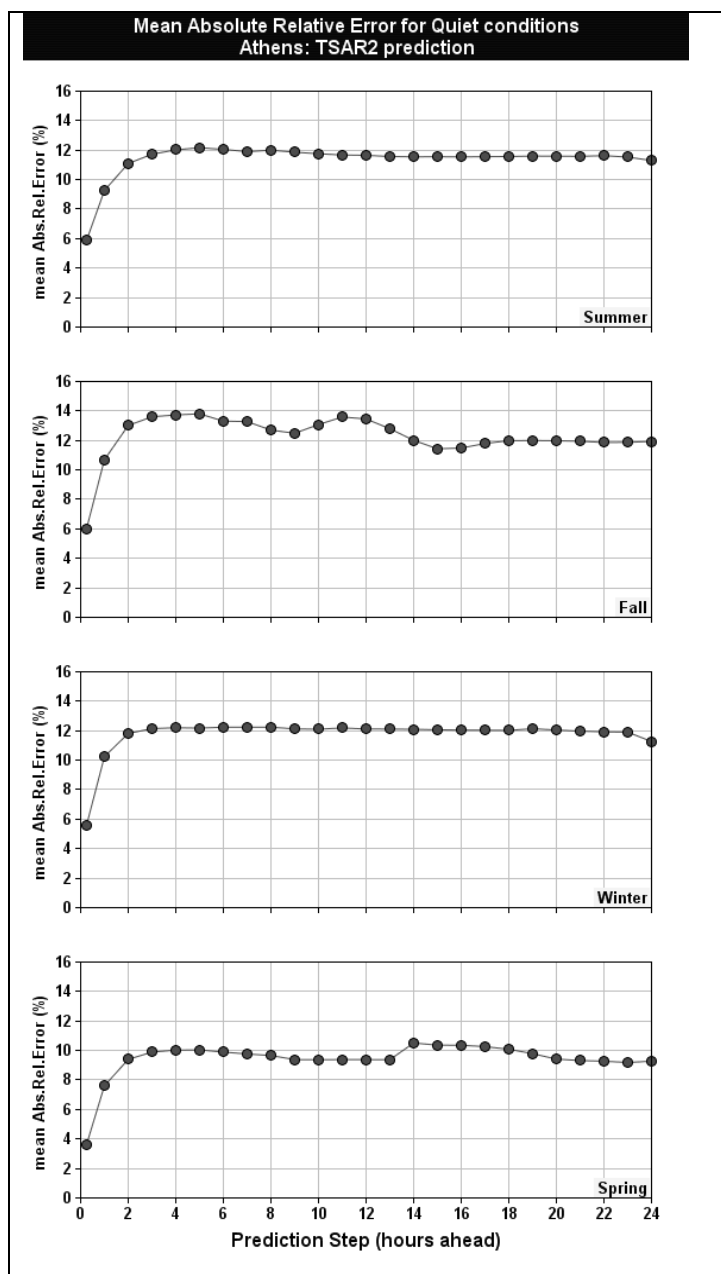


Figure 11: *The mean absolute relative error estimates for Athens as a function of the prediction step (1-24 hours ahead) for each season.*

The TSAR performance is not successful during storm intervals. We analyzed the TSAR performance using data from Athens Digisonde during four storm events of moderate to intense intensity occurred in the following time intervals: 28 August 2004 – 5 September 2004 (first storm event), 21 – 31 January 2004 (second storm event), 2 – 5 April 2004 (third storm event) and 5-9 April 2004 (fourth storm event).

To quantify the relative performance of the two methods, the mean absolute relative error over the three phases of each storm (initial, main and recovery) was calculated for all storm events (Figure 12) for Athens location. The first remark from the inspection of these results is that the prediction efficiency of both methods becomes poorer for longer prediction time horizon (up to six hours). In addition, the poorer performance of TSNN method with respect to TSAR for a prediction horizon greater

than 1 hr, is clearly demonstrated with the statistical analysis shown in Figure 12.

In respect to the storm development, the mean absolute relative error with TSAR method is rather small during the initial phase of the storm, with a general tendency to increase as the storm evolves and recovers. This is rather expected since the methods' predictions are based on the most recent measurements, which progressively include more and more disturbed data as we move to the end of the storm.

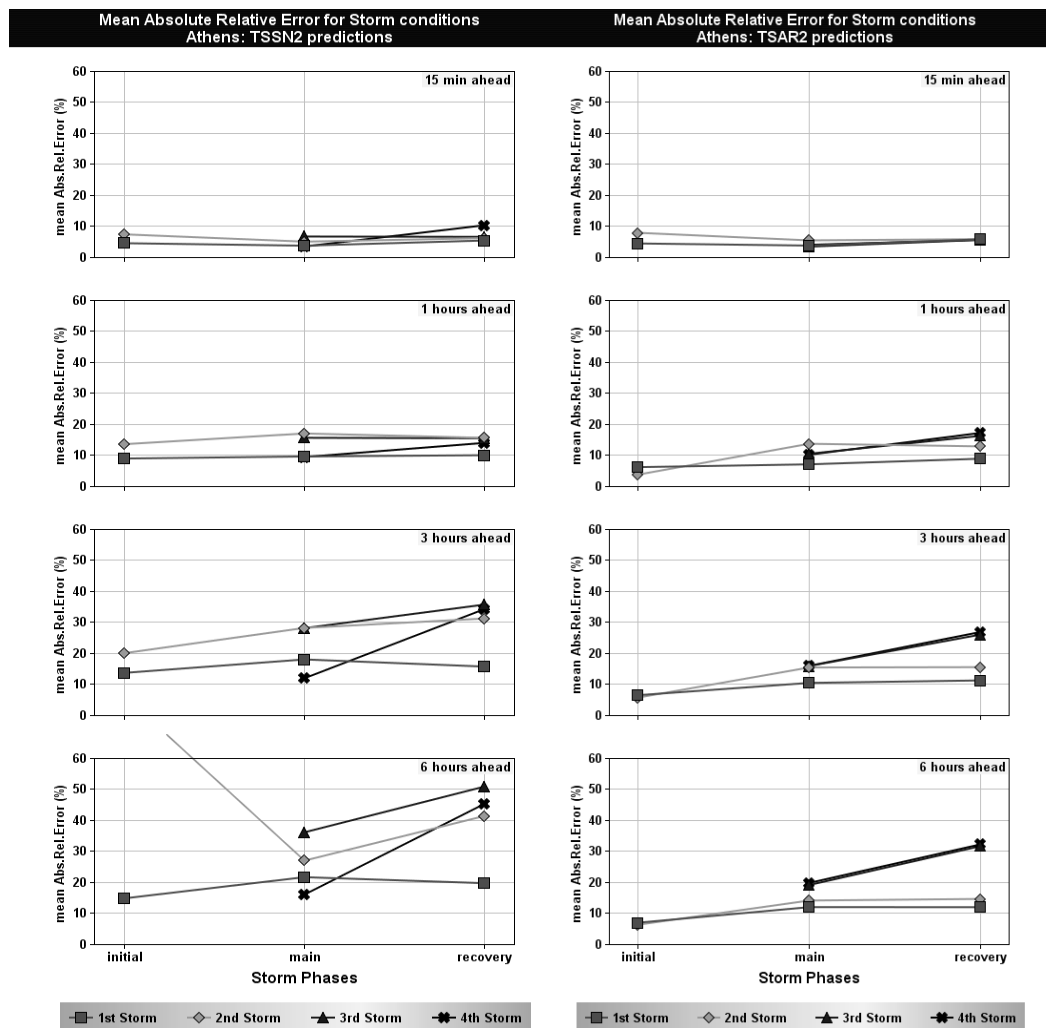


Figure 12: The mean absolute relative error values for Athens location and for prediction windows 15min, 1hr, 3hrs and 6hrs calculated over the three phases of each storm (initial, main and recovery) using the prediction results of the two methods TSNN2 (left), and TSAR2 (right).

In general, according to the results,

- TSAR method provides very successful results for predictions 15 min and 1 h ahead and statistically reliable results for predictions up to 24 hours ahead especially for quiet conditions.
- The prediction efficiency of the method becomes poorer for longer prediction time horizon.
- During storm intervals, the prediction error is rather small during the initial phase of the storm, with a general tendency to increase as the storm evolves and recovers, indicating that the use of TSAR for ionospheric forecasting purposes during storms is not the adequate method.

b) Comparative evaluation between STIM and TSAR

The two methods' (TSAR and STIM) performance was comparatively evaluated over Athens location during six intense ($Dst \leq -100$ nT) storm events, listed in Table 6.

Table 6: List of storm events used for this part of the analysis

Time Interval	Min Dst (nT)
19-22 March, 2001	-149
17-23 April, 2002	-149
3-6 September, 2002	-109
29-31 May, 2003	-144
30 August-1 September, 2004	-126
12-15 June, 2005	-106

Actual observations were first compared with the two method's predictions and the results are presented in Figure13 for TSAR's predictions and in Figure14 for STIM's predictions. TSAR's predictions for different prediction step (1, 3, 6, and 24h ahead) are analyzed separately. The results are also grouped into three columns, following roughly the day-to-day ionospheric storm development. Three days are distinguished: the pre-storm day which corresponds to quiet conditions prior to the ionospheric storm onset, the main storm day when intense storm-time ionospheric disturbances are recorded and the post-storm day which mainly includes the recovery to normal conditions.

According to the results presented in Figure 13, three main points are revealed: i) TSAR's predictions for 1h ahead are successfully correlated with actual observations under all possible ionospheric conditions, ii) during pre-storm conditions the TSAR' predictions are well correlated with actual observations for all prediction steps up to 24h ahead and iii) during storm conditions and for prediction steps greater than 1h ahead, TSAR's predictions significantly deviate from the observed values, while the deviation is further increased during the day that follows the ionospheric disturbance. On the other hand, STIM's predictions (Figure 14) are satisfactory correlated to the observed foF2 values during all days. The two methods' performance appears to be

comparable at all aspects during pre-storm conditions, but significant discrepancies arise during storm and post-storm conditions. STIM systematically yield in better results than TSAR especially when the prediction step of the latter becomes greater than 1h ahead.

To quantify the deviation of the two methods predictions from the observed values, the RMSE for each day of the selected storm-time intervals was calculated and the averages over all events are presented in Figure15. The averaged RMSE is around 1 MHz during all storm days for STIM's and TSAR's – 1h ahead predictions while it increases up to about 2 MHz during the main storm day for TSAR's predictions from 3 to 24h ahead.

The evaluation of performance of TSAR against STIM during storms can be summarized as follows: i) TSAR provides successful predictions for prediction steps from 1h ahead, ii) for prediction steps from 3 h to 24 h ahead, STIM's performance is systematically more successful than TSAR's and iii) TSAR is not able to follow the ionospheric response during the storm onset and recovery, while STIM can capture the physical processes that govern the ionospheric storm onsets and their temporal evolution.

2.2 The synthesis of SWIF model

The above analysis indicates that TSAR's predictions can take substantial advantage from the output of the STIM method during storm conditions and were taken into account in the development of a preliminary version of the integrated SWIF algorithm that combines STIM's and TSAR's predictions during storm conditions. Storm conditions are determined by STIM's alert signal. In the absence of an alert signal, SWIF performs like TSAR. A diagram showing the SWIF synthesis is presented in Figure 16.

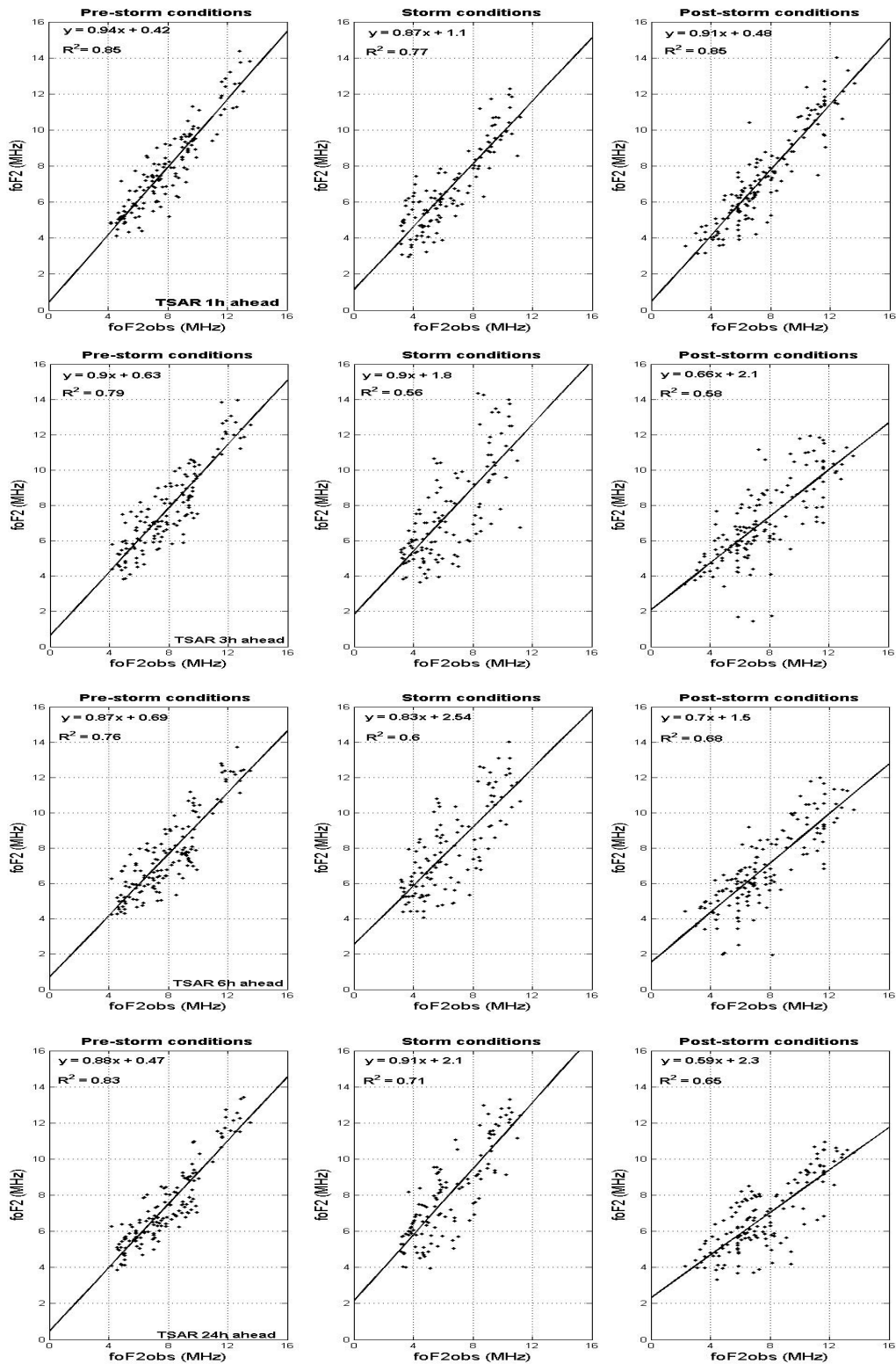


Figure 13: TSAR's predictions in respect to actual observations for the six storm time intervals listed in Table 1 and for various prediction steps: 1h ahead (first panel), 3h ahead (second panel), 6h ahead (third panel) and 24 h ahead (last panel). The results are grouped into three columns, one for each storm day: the pre-storm, the main storm and the post-storm day. The regression line and its equation are also plotted in each case.

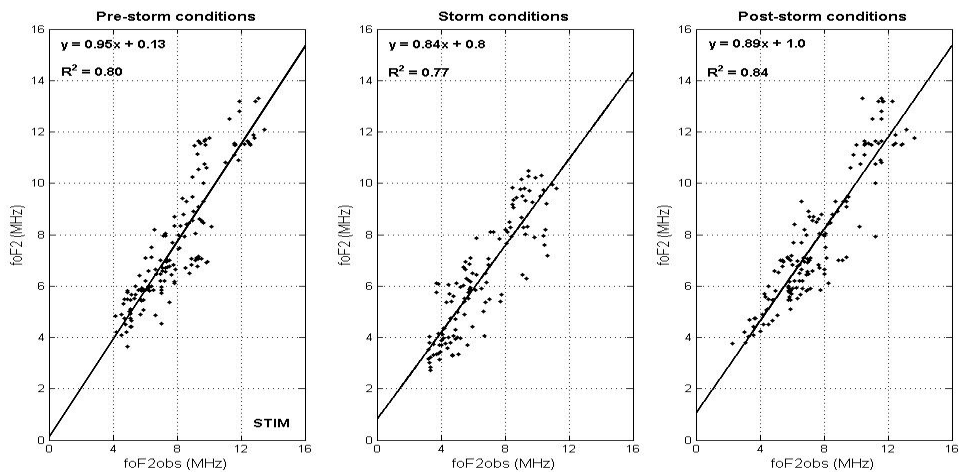


Figure 14: STIM's predictions in respect to actual observations for the six storm time intervals listed in Table 1. The results are grouped into three columns, following roughly the day-to-day ionospheric storm development. Three days are distinguished: the pre-storm day, the main storm day post-storm day. The regression line is also plotted in each case.

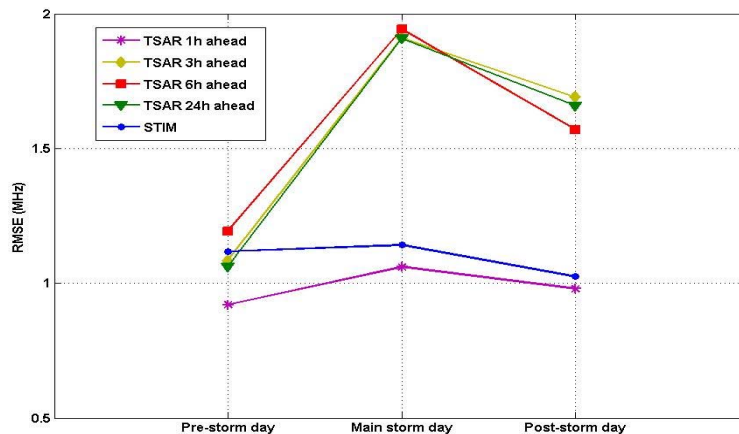


Figure 15: The averaged RMSE per storm day over all the events listed in Table 1.

In summary, SWIF's main components for storm cases can be described as follows:

- For predictions 1h ahead, TSAR's predictions are provided in all cases.
- For prediction window greater than 1h ahead the SWIF algorithm first determines the onset and the end of the ionospheric storm disturbance by using STIM's output based on: i) the alert signal obtained from the online analysis of the IMF observations provided from ACE, ii) the empirical formulation of the ionospheric storm-time response considering the LT and the latitude of the observation point. STIM's predictions are provided by SWIF algorithm for the whole of the ionospheric storm duration as well as for 24 hours after its end.
- SWIF recovers the full set of TSAR's predictions 24 hours after the end of the ionospheric storm disturbance.

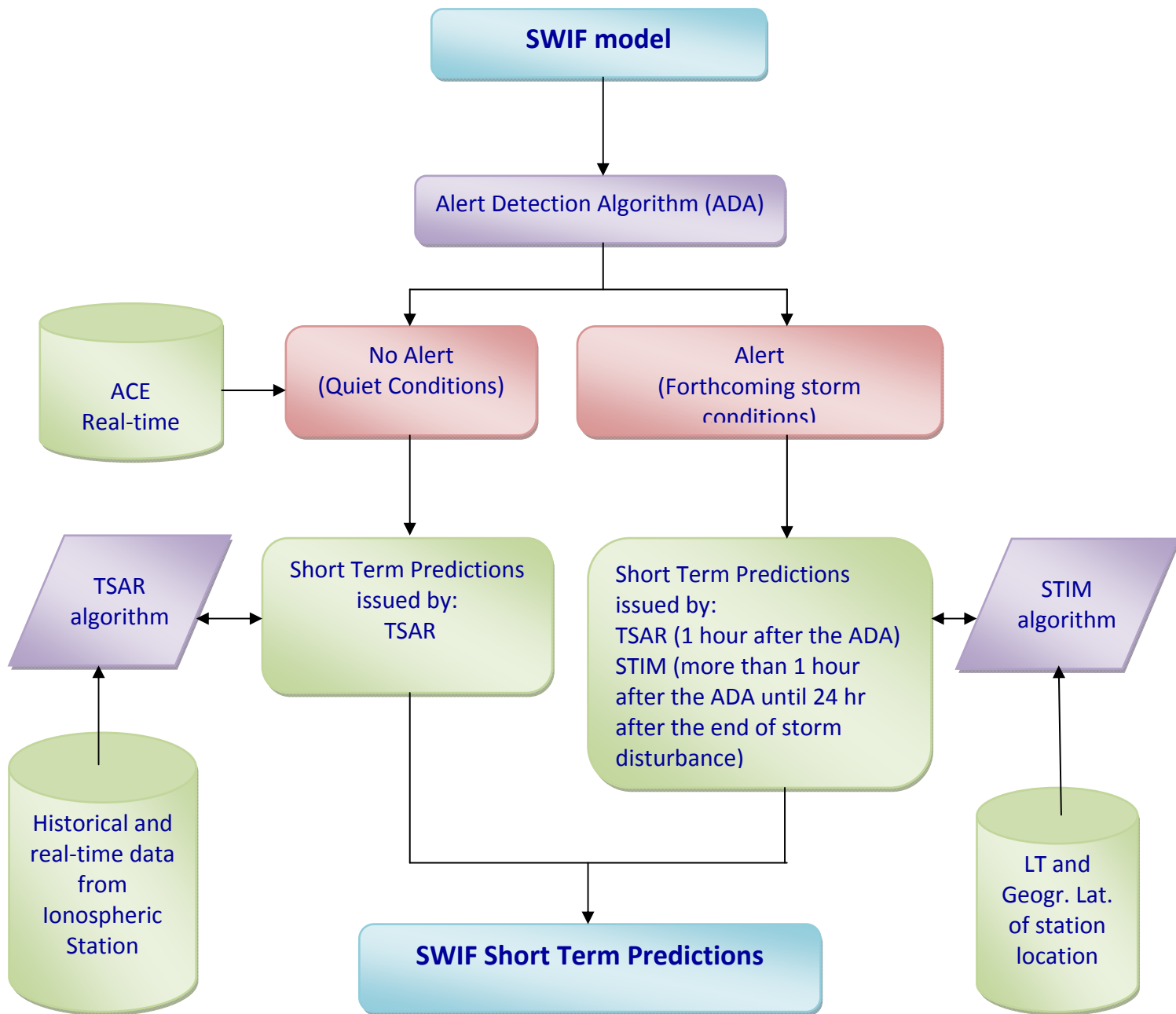


Figure 16: Diagram showing the SWIF synthesis.

2.3 Evaluation of SWIF performance

The predictions of SWIF algorithm are evaluated in terms of actual observations from Athens Digisonde and the predictions of the Geomagnetically Correlated Autoregression Model (GCAM) introduced by Muhtarov et al. (2002). The predictive variable is the deviation of the foF2 parameter from the monthly median values, given by:

$$\delta = \frac{f_oF2 - f_oF2_{median}}{f_oF2_{median}}$$

The general form of the cross correlation model is:

$$\Phi_0 = \bar{\Phi} + \sum_{k=1}^n \beta_k (\Phi_k - \bar{\Phi}) + \sum_{k=0}^n \gamma_k (G_k - \bar{G})$$

We consider n measured values Φ_i at times t_i ($i=1, \dots, n$) ordered in decreasing time, and look for the value of Φ_0 at time t_0 .

For the same times t_i we have n+1 values of a geomagnetic index G_i ($i=0, 1, 2, 3, \dots, n$).

β_k and γ_k are weighting coefficients for each $k=0, 1, \dots, n$ and $\bar{\Phi}$ and \bar{G} are the mean values of Φ and G .

$\sum_{k=1}^n \beta_k (\Phi_k - \bar{\Phi})$: This part depends on the past n values of Φ .

$\sum_{k=0}^n \gamma_k (G_k - \bar{G})$: This part depends on the past n values and on the value for the time of prediction of the magnetic activity index G .

In GCAM, a synthetic geomagnetic index (G) and its statistical characteristics was added to an autocorrelation model, improving significantly its prediction capability. SWIF and GCAM algorithms share in some way the same approach to the ionospheric forecasting issue, and therefore the comparison between SWIF's and GCAM's predictions is considered as the best indicator for SWIF's performance.

a) Evaluation of prediction efficiency under quiet intervals

The comparison of the two models' performance has been done for the Athens Digisonde site, based on post-event analysis with autoscaled data during geomagnetically quiet and disturbed intervals from 2001 to 2007. Here it is necessary to remind the reader that during quiet conditions SWIF algorithm provides TSAR's predictions. The results are summarized in Figure 17 for geomagnetically quiet intervals during fall season. In general the GCAM performs more successfully than TSAR at least for the first 12 hours. The autoscaling of the ionograms during the first interval (1-20 October 2005) is performed with ARTIST4.0 software, while for the second interval (1-20 October 2007) the ionograms have been autoscaled with the upgraded ARTIST4.5 (Reinisch et al., 1983; 2005). In Figure 18 we present the analysis of the GCAM and TSAR performance during summer time quiet intervals (1-30 June 2004 and 1-20 June 2007). The results show in general that both models are sensitive to the quality of the data sample (gaps and ionograms scaling performance) used to derive the foF2 prediction (previous 96 hours for GCAM; previous two months for TSAR). However the quality of the autoscaling software (ARTIST) performance determines largely the accuracy of the TSAR results and in a smaller degree the accuracy of GCAM.

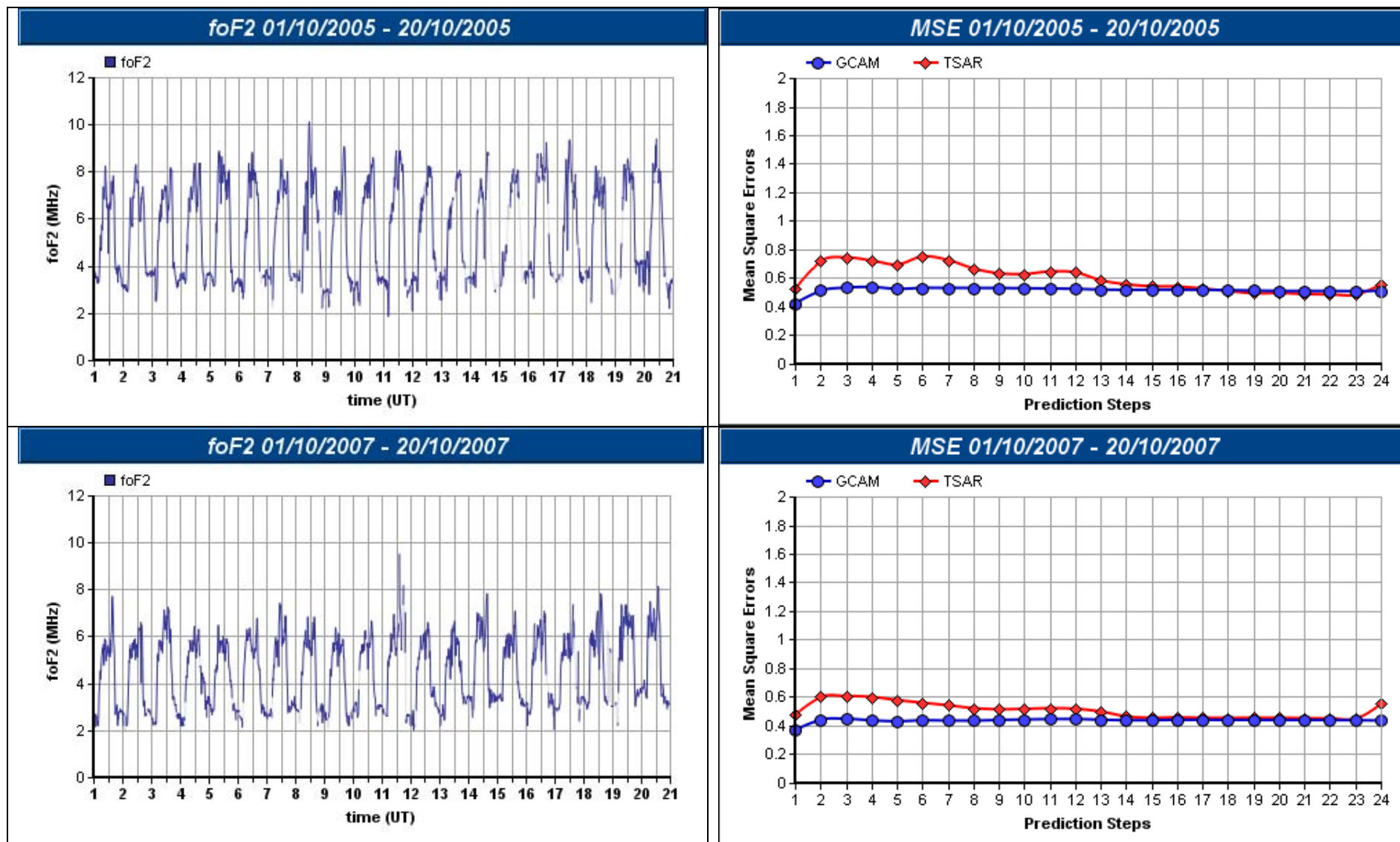


Figure 17: Athens Digisonde ionograms autoscaled with ARTIST4.0 (top) and with ARTIST4.5 (bottom) during fall quiet intervals

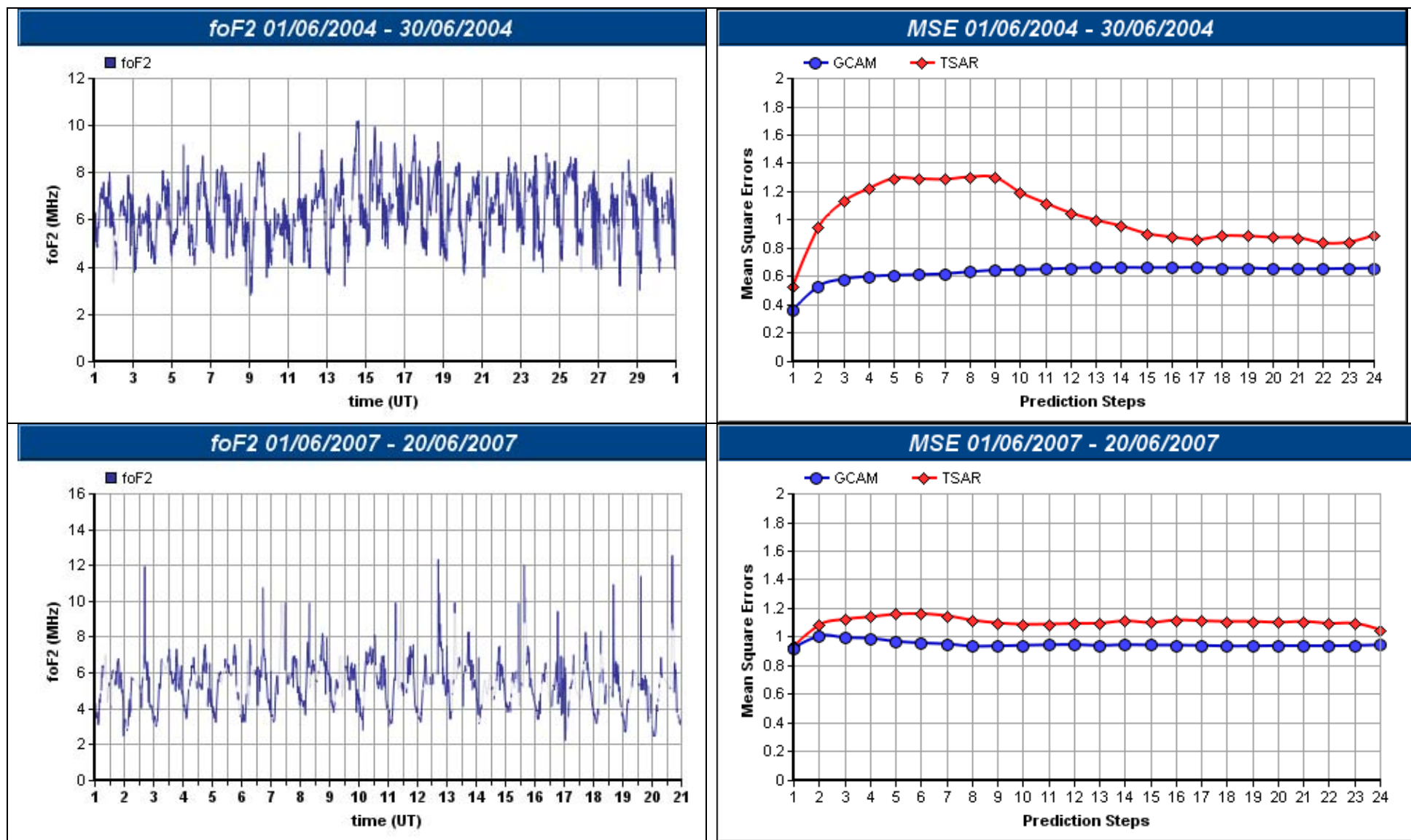


Figure 18: Athens Digisonde ionograms autoscaled with ARTIST4.0 (top) and with ARTIST4.5 (bottom) during summer quiet intervals

b) Evaluation during storm conditions

The predictions obtained from GCAM and SWIF were compared with actual observations obtained from Athens digisonde. All available observations for the storm events listed in Table 4 were used for this part of the analysis and the results are presented in Figure 19.

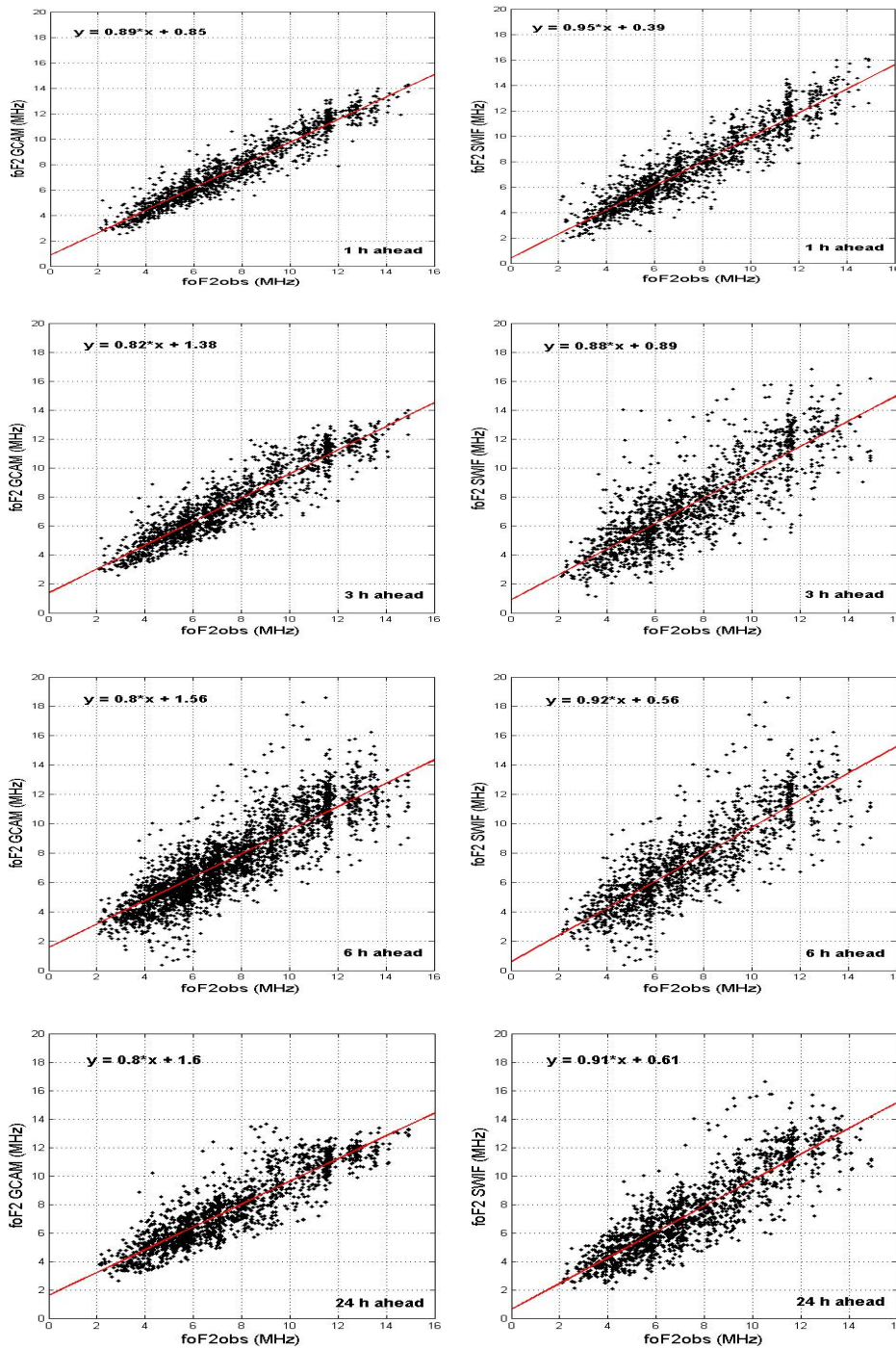


Figure 19: Comparison of SWIF and GCAM predictions during the storm events listed in Table 4

The relative errors between SWIF's and GCAM's predictions and actual observations obtained from Athens digisonde were also evaluated using two error parameters e_1 and e_2 : $e_1 = |\text{foF2}_{\text{obs}} - \text{foF2}_{\text{GCAM}}|/\text{foF2}_{\text{obs}}$ and $e_2 = |\text{foF2}_{\text{obs}} - \text{foF2}_{\text{SWIF}}|/\text{foF2}_{\text{obs}}$. The scatter plots of e_2 versus e_1 obtained for all storm events are shown in Figure 20, separately for different prediction steps. The best fit line is over plotted in each diagram. In all cases the criterion $e_1 < e_2$ is always satisfied and the correlation coefficient is less than the unit in all cases, providing strong evidence for better performance of SWIF over GCAM. The prediction efficiency (Kutiev and Muhtarov, 2001), P_{eff} , was also estimated in all cases. The prediction efficiency shows the gain of the accuracy of a model compared with some reference model. Here we verify once again that SWIF performance is more successful than GCAM in all cases. For predictions 1h ahead, SWIF gains 28% of accuracy in respect to GCAM, while the prediction efficiency increases to 57% for predictions 3h ahead and reaches 61% and 59% for predictions 6h and 24h ahead, respectively.

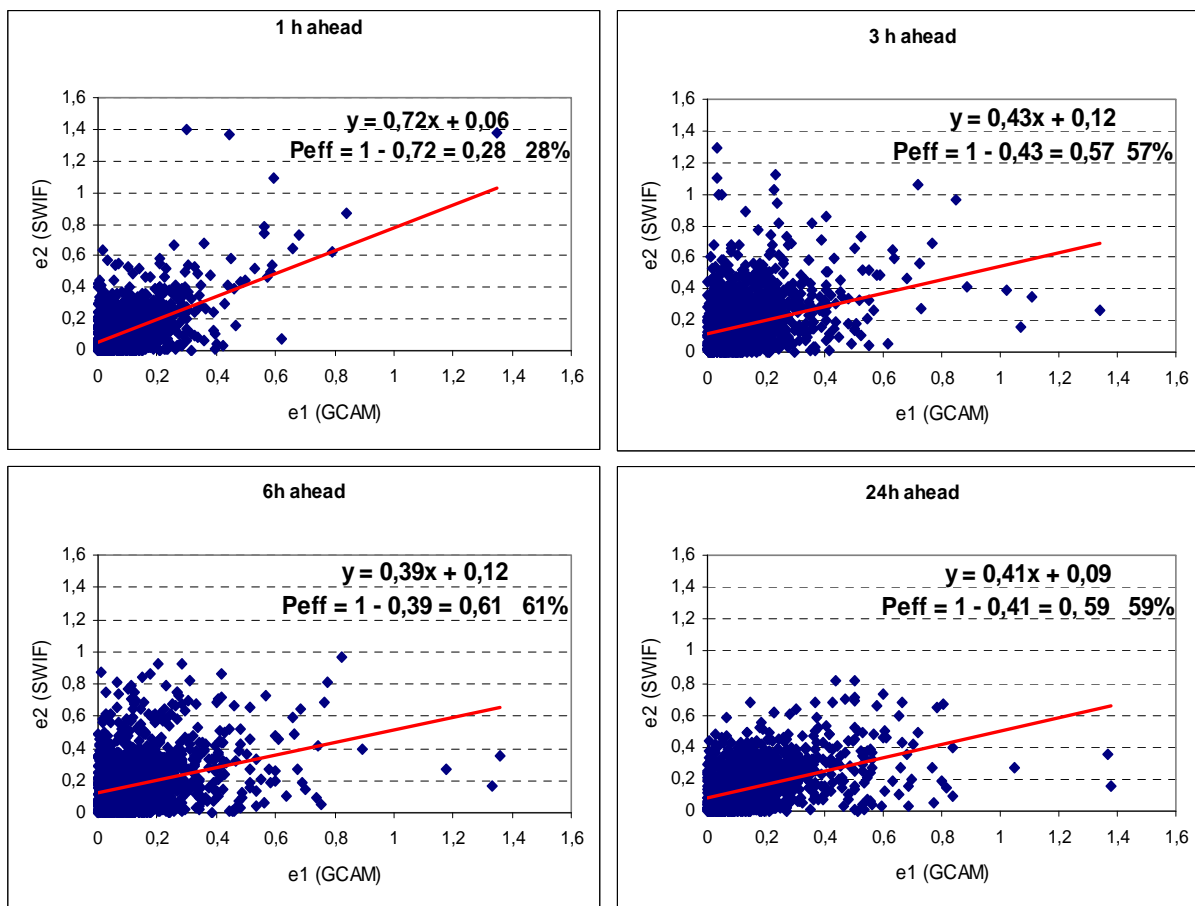


Figure 20: Scatter plots of e_2 versus e_1 for the time intervals analysed in this part of the analysis. The regression line and its equation are also shown, together with the estimated prediction efficiency, P_{eff} .

3. The on-line tool for the operational use of SWIF model

The SWIF model has been implemented on-line and the results for Athens station are available in the address <http://195.251.203.13/ACE/CurrentACE/CurrentACE.html>.

This on-line tool consists on the development of three algorithms:

- a) The storm detection algorithm which, based on the analysis of interplanetary magnetic field data from ACE satellite, calculates the required parameters (see section 1.1.1) and issues alert signal for forthcoming disturbances from the solar wind. The whole procedure is demonstrated in Figure 21.
- b) The TSAR algorithm (see section 2.1) that provides ionospheric forecasts up to 24 hours ahead under the condition that there is no alert for forthcoming disturbances.
- c) The STIM algorithm, which is activated after the issuing of an alert signal (see section 1.1.3 and 2.2) and provides forecasts within the duration of the storm.

The user of this service has access to the following features:

- a) Time plot of the ionospheric parameter foF2 for the past 24 hours
- b) Time plot of the monthly median values of the foF2 parameter for the past and the next 24 hours
- c) Time plot of the foF2 forecasting values using the SWIF model for the next 24 hours
- d) Time plot of the foF2 forecasting parameters using the GCAM model for the next 24 hours
- e) Time plot of the interplanetary magnetic field parameters (IMF-B, IMF-Bz, IMF-dB/dt), obtained from ACE satellite, for the past 24 hours
- f) The current IMF conditions in ASCII values
- g) Indication of current alert conditions
- h) The forecasted foF2 parameters for the next 24 hours, with GCAM and SWIF models, in ASCII format, together with the monthly median values of the foF2 parameter.

Two viewgraphs of the SWIF implementation tool are shown in Figures 22 and 23, for quiet and disturbed conditions respectively.

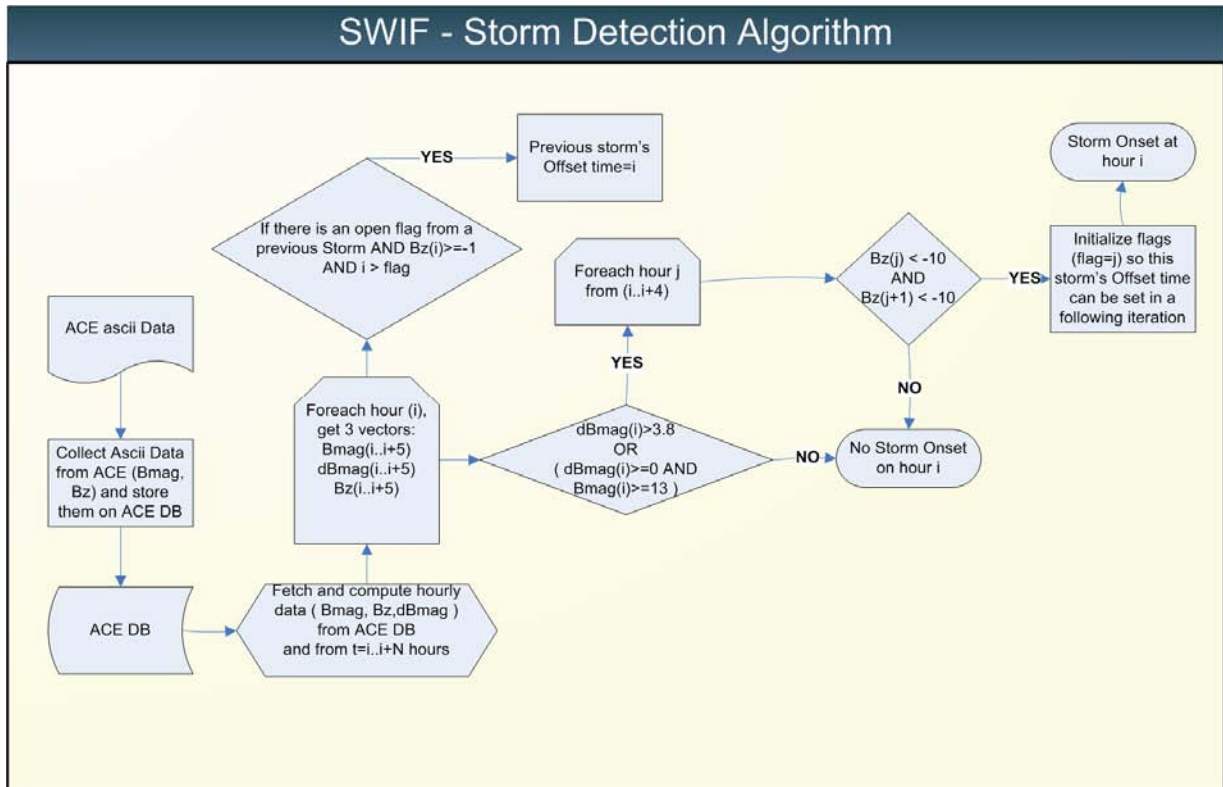


Figure 21: The storm detection algorithm applied for SWIF on-line implementation, using real-time data from ACE satellite (<http://www.swpc.noaa.gov/ftplib/lists/ace/>)



NOA Ionospheric Predictions over Athens

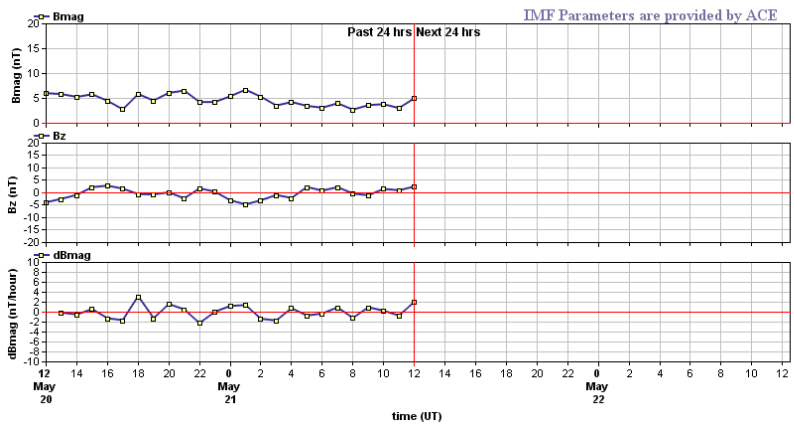
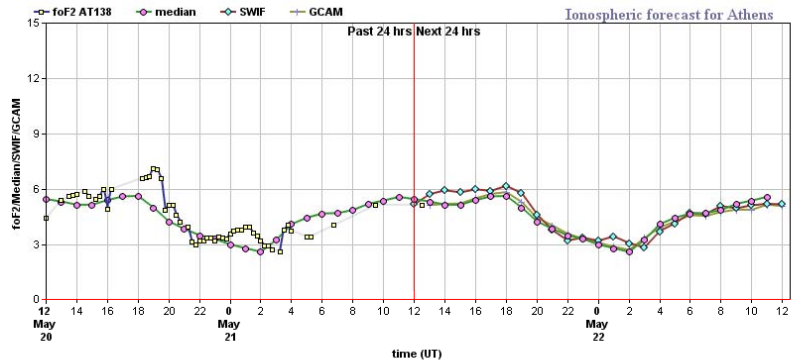
SWIF
"Solar Wind driven autoregression model for ionospheric short term Forecast"
The SWIF Project was funded by EOARD



ACE Nowcasting at 21/05/2008 12:00

Bmag	4.93
Bz	2.34
dBmag	1.97

No Storm Alert



Display Data

On line Documentation

Logout

Refresh

Figure 22: On-line SWIF implementation results under quiet conditions



NOA Ionospheric Predictions over Athens

SWIF
 "Solar Wind driven autoregression model for Ionospheric short term Forecast"
 The SWIF Project was funded by EOARD

ACE Nowcasting at 11/02/2004 12:00

Bmag	13.60
Bz	-11.31
dBmag	0.44
Storm Alert	

Storm Characteristics:

No	Storm Onset	Storm End	Ionospheric Storm Onset	Ionospheric Storm End	Predicted Effect	Max foF2 deviation
0	11/02/2004 11:00	11/02/2004 18:00	11/02/2004 19:00	12/02/2004 18:00	negative	-49.57 %

Display Data

On line Documentation

Logout

Refresh

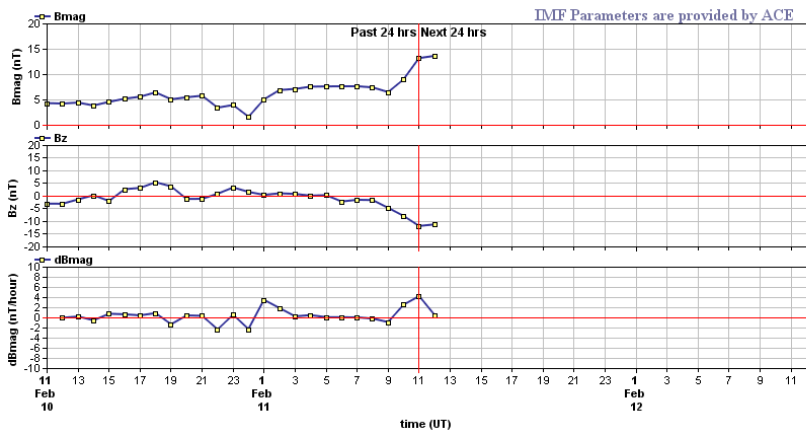
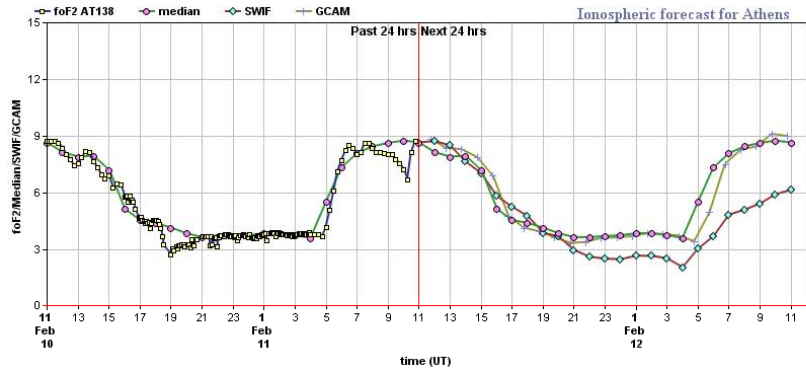


Figure 23: On-line SWIF implementation results under storm conditions

4. Conclusions and the way ahead

This project is devoted to a very important and challenging problem – short-term foF2 prediction during severe geomagnetic storms. Despite long history and lots of attempts undertaken there is not much progress in this direction. This is due to a great complexity of the problem when many competing processes turn out to be involved and the efficiency each of them is not controlled.

In practice, the ionospheric forecast is widely approached by empirical methods which are based on the correlation of the ionospheric disturbances with various geophysical indices (e.g. Fuller-Rowell et al., 2000; Muhtarov et al., 2002; Mikhailov et al., 2007). However, there is no efficient geophysical index to predict the ionospheric storm onset, its magnitude and duration (Mikhailov et al., 2007) and therefore the ionospheric forecast remains an unsolved and very challenging problem.

Based on recent advances in ionospheric storm dynamics, which correlate the ionospheric storm effects with solar wind parameters (for example Davis et al., 1997; Watanabe et al., 2000; Belehaki and Tsagouri, 2002) such as the magnitude and the orientation of the interplanetary magnetic field (IMF) and on the availability of these parameters in real time by the ACE spacecraft from the vantage L1 point, an new end-to-end short-term ionospheric prediction service, the SWIF, was envisaged and developed in the frames of this project. Because it takes about an hour for the solar wind to travel from where ACE is, in L1 point, to the Earth, telemetry from ACE allows alerts of geospace storms to be issued nominally an hour in advance of their occurrence effects to geospace environment (Kappenman, 1998).

SWIF is based on the fusion of two diverse techniques, an autoregression forecasting algorithm (TSAR) capable for real time predictions and the empirical STIM method for predicting the onset and for scaling ionospheric disturbances during geomagnetic storms based on the solar wind parameters.

According to our results, the TSAR method provides very successful results for predictions 15 min and 1 h ahead and statistically reliable results for predictions up to 24 hours ahead especially for quiet conditions. During storm intervals, the prediction error is rather small during the initial phase of the storm, with a general tendency to significantly increase as the storm evolves and recovers. On the other hand, STIM is designed to scale the ionospheric storm-time response, providing ionospheric predictions from 18 to 40 hours ahead. Validation tests of the methods predictions during a significant number of storm events gave evidence for statistically accurate predictions during all storm phases. In particular, STIM proved able to successfully capture the physical processes that govern the ionospheric storm onsets and their temporal evolution from the onset towards the recovery, providing improved forecasts in comparison to monthly median values.

All the above indicate that TSAR's predictions could take substantial advantage from the output of the STIM method at least during transitional periods such as the onset and the recovery of a storm event. The two methods' cooperation combined in SWIF model has been extensively tested during quiet and storm periods and compared with the GCAM performance showing a clear improvement in forecasting efficiency especially during storm conditions.

The approach proposed here is based on a clear idea that IMF parameter variations via the chain of processes result with a certain time delay in ionospheric F2-layer storms. SWIF succeeds to

predict successfully a general ionospheric pattern that follows a geomagnetic storm at middle latitudes.

SWIF is implemented on line and the forecasts are accessible in real-time through the web address: <http://195.251.203.13/ACE/CurrentACE/CurrentACE.html>. The current implementation provides the SWIF predictions over Athens station. Immediate future developments might include:

- a) Application of SWIF procedure to all middle latitude European stations participating in DIAS system (Belehaki et al., 2006; 2007c). DIAS (The European Digital Upper Atmosphere Server) provides nowcasts and forecasts for ionospheric conditions over Europe and has been jointly developed by 8 European Universities and Research Institutes (<http://www.iono.noa.gr/DIAS>) and currently operated by the National Observatory of Athens (<http://dias.space.noa.gr>)
- b) Based on the application of SWIF procedure to all DIAS stations we will be able to develop a database which will be very useful for evaluation of SWIF performance with emphasis on latitudinal and seasonal effect on the forecasting efficiency. This will also give us the possibility for analytical studies concerning the effect of transient or irregular patterns, such as the sporadic E-layer, to the prediction efficiency of SWIF.

It is worthy to note that DIAS system currently serves more than 100 subscribed users, among which we can refer to ONERA French Aerospace Lab (France), GFZ Potsdam (Germany), IPGP Institut de physique du globe de Paris (France), IZMIRAN Pushkov Institute of Terrestrial Magnetism (Russia), BBC (UK), University of Massachusetts Lowell (USA), NOAA National Oceanic & Atmospheric Administration (USA), National Centre for Atmospheric Research (USA), NASA Marshall Space Flight Center (USA), NASA Jet Propulsion Laboratory (USA), IPS Radio and Space Services (Australia), University of Liège (Belgium), Chinese Academy of Sciences, Institute of Geology and Geophysics (China), University Rennes I (France), Institute of Methodologies for Environmental Analysis, CNR (Italy), Rostov State University (Russia), Polar Geophysical Institute, Russian Academy of Sciences (Russia), Universidad Complutense de Madrid (Spain), University of Bath (UK), CERN (Switzerland), University of Lancaster (UK), University of Alabama in Huntsville (USA), Clemson University (USA), George Mason University (USA). The upgrade of DIAS system based on the directions analyzed above will critically support the large number of researchers and users worldwide seeking for accurate ionospheric nowcasting and forecasting services, and will consist a very important step forward concerning the very challenging and complicated problem of ionospheric short term prediction.

References

- Araujo-Pradere, E., Fuller-Rowell, T.J. STORM: An empirical storm-time ionospheric correction model 2. Validation. *Radio Sci.*, 37, 10.1029/2002RS002620, 2002.
- Belehaki A., and I. Tsagouri, On the occurrence of storm induced nighttime ionization enhancements at ionospheric middle latitudes, *J. Geophys. Res.*, 107, 8, 22, 2002.
- Belehaki A., Lj. Cander, B. Zolesi, J. Bremer, C. Juren, I. Stanislawska, D. Dialetis and M. Hatzopoulos, Monitoring and forecasting the ionosphere over Europe: The DIAS project, *Space Weather*, 4, S12002, doi:10.1029/2006SW000270, 2006.
- Belehaki, A., I. Tsagouri and K. Koutroumbas, First Interim Report, EOARD Contract FA8655-07-M-4008, September 2007a
- Belehaki, A., I. Tsagouri and K. Koutroumbas, Second Interim Report, EOARD Contract FA8655-07-M-4008, November 2007b
- Belehaki, A., Lj. Cander, B. Zolesi, J. Bremer, C. Juren, I. Stanislawska, D. Dialetis and M. Hatzopoulos, Ionospheric specification and forecasting based on observations from European ionosondes participating in DIAS project, *Acta Geophysica*, Volume 55, 3, doi: 10.2478/s11600-007-0010-x, pp 398-409, 2007c
- Davis, C.J., Wild, M.N., Lockwood, M., and Tulunay, Y.K., Ionospheric and geomagnetic responses in IMF Bz: a superposed epoch study, *Ann. Geophysicae*, 15, 217-230, 1997.
- Fuller-Rowell, T.J., Codrescu, M.V., Moffett, R.J., and Quegan S., Response of the thermosphere and ionosphere to geomagnetic storms. *J. Geophys. Res.*, 99, 3893-3914, 1994.
- Fuller-Rowell, T.J., Araujo-Pradere, E., Codrescu, M.V. An empirical ionospheric storm-time correction model. *Adv. Space Res.*, 25(1) 139-146, 2000.
- Fuller-Rowell, T.J., Codrescu, M.V., Rishbeth, H., Moffett, R.J., and Quegan S., On the seasonal response of the thermosphere and ionosphere to geomagnetic storms. *J. Geophys. Res.*, 101, 2343, 1996.
- Gonzalez W.D., and Tsurutani, B.T., Criteria of interplanetary parameters causing intense magnetic storms ($Dst < -100$ nT), *Planetary Space Sci.*, 35, 1101, 1987.
- Gonzalez W.D., Tsurutani, B.T. and Gonzalez A.L., Interplanetary origin of geomagnetic storms, *Space Science Reviews*, 88, 529-562, 1999.
- Gonzalez WD, de Gonzalez ALC, Sobral JHA, Dal Lago A and Vieira LE., Solar and interplanetary causes of very intense geomagnetic storms, *J. Atmos. Solar Terr. Phys.* 63 (5): 403-412 MAR 2001
- Kappenman, J.G. Geomagnetic storm forecasting mitigates power system impacts. *IEEE Power Engineering review*, 18, N. 11, 1998.
- Koutroumbas K., I. Tsagouri and A. Behlaki, Time series autoregression technique implemented on-line in DIAS system for ionospheric forecast over Europe, *Annales Geophysicae*, 26(2), 371-386, 2008.

- Koutroumbas, K. and A. Belehaki, "One-step ahead prediction of $foF2$ using time series forecasting techniques", *Annales Geophysicae*, Vol. 23, pp. 3035-3042, 2005.
- Mikhailov A.V., Depuev V.H., and Depueva A.H., Short-term foF2 forecast: Present day state of art, in *Space Weather: Research towards applications in Europe*, Astrophysics and Space Science Library, 344, 169-184, 2007.
- Muhtarov, P., I. Kutiev, and L. Cander, Geomagnetically correlated autoregression model for short-term prediction of ionospheric parameters, *Inverse Problems*, 18, 49-65, 2002.
- Prölss, G.W., On explaining the local time variation of ionospheric storm effects, *Ann. Geophys.*, 11, 1-9, 1993.
- Reinisch, B.W., X. Huang, I.A. Galkin, V. Paznukhov, A. Kozlov, Recent advances in real-time analysis of ionograms and ionospheric drift measurements with digisondes, *Journal of Atmospheric and Solar-Terrestrial Physics* 67, 1054–1062, 2005
- Reinisch, B.W., Huang, X., Automatic calculation of electron density profiles from digital ionograms, 3, *Processing of bottomside ionograms*, *Radio Science* 18, 477–492, 1983
- Tsagouri I. and Belehaki A.: A new empirical model of middle latitude ionospheric response for space weather applications, *Advances in Space Research*, 37, 420-425, 2006.
- Tsurutani, B.T., and Gonzalez W.D., The future of geomagnetic storm predictions: implications from recent solar and interplanetary observations, *J. Atmospheric Terrest. Phys.*, 57, 1369, 1995.
- Watanabe M., N. Sato, R.A. Greenwald, M. Pinnock, M.R Hairston, R.L. Raisen and D.J. McEwen, The ionospheric response to interplanetary magnetic field variations: Evidence for rapid global change and the role of preconditioning in the magnetosphere, *J. Geophys. Res.*, 105, 22955, 2000.